Australian Laterites Reveal Mechanisms Governing Scandium Dynamics in the Critical Zone

Mathieu Chassé, William L Griffin, Suzanne y O'Reilly, Georges Calas

Australian Laterites Reveal Mechanisms Governing Scandium Dynamics in the Critical Zone

Mathieu Chassé[a,b,*], William L. Griffin[b], Suzanne Y. O'Reilly[b], Georges Calas[a]

[a] *Sorbonne Université, Muséum national d'Histoire naturelle, UMR CNRS 7590, IRD, Institut de minéralogie, de physique des matériaux et de cosmochimie (IMPMC), F-75005 Paris, France*

[b] *Australian Research Council Centre of Excellence for Core to Crust Fluid Systems (CCFS) and GEMOC, Department of Earth and Planetary Sciences, Macquarie University, NSW 2109, Australia*

Abstract

Scandium is often considered as immobile during chemical weathering, based on its low solubility. In contrast to other conservative (*i.e.* relatively immobile) elements incorporated into accessory minerals resistant to weathering (*e.g.* zirconium, thorium or niobium), the scarcity of scandium minerals indicates that the processes accounting for scandium's immobilisation are distinctive. However, the evolution of scandium speciation during weathering is unknown, limiting the understanding of the processes controlling its dynamics in the critical zone. Exceptional scandium concentrations in east Australian laterites provide the possibility of unravelling these mechanisms. We follow scandium speciation through thick lateritic profiles (> 30 m) using a multiscale mineralogical and spectroscopic approach involving electron microprobe, laser-ablation–inductively coupled plasma mass spectrometry, selective leaching and X-ray absorption near-edge structure spectroscopy, complemented by mass-transfer calculations. We show that the initial reservoir of scandium contained in the parent rock is preserved under reducing conditions occurring in the lowest horizons of the profiles. The dissolution of scandium-bearing clinopyroxene generates smectitic clays that immobilise and concentrate scandium. It is subsequently trapped in the lateritic duricrust by goethite. Scandium mobilisation appears in this horizon and increases upward as a result of the dissolution of goethite, possibly assisted by dissolved organic matter, and the precipitation of hematite. Molecular-scale analyses demonstrate that changes in speciation govern scandium dynamics, with substitution in smectitic clays and adsorption on iron oxyhydroxides playing a crucial role in scandium immobility in the saprolite and lower lateritic duricrust. The higher affinity of scandium for goethite relative to hematite drives scandium mobilisation in the upper lateritic duricrust, leading to its concentration downward in the lower lateritic duricrust. These successive mechanisms illustrate how the unique complexity of the critical zone leads to scandium concentrations that may form new types of world-class scandium deposits. Comparison with conservative elements and with rare-earth elements, expected to have similar geochemical properties, emphasizes the unique behaviour of scandium in the critical zone. While scandium remains immobile during the early stages of weathering, intense and long-term alteration processes, observed in lateritic contexts, lead to scandium mobilisation. This study highlights the dependence of scandium mobility on weathering conditions.

Keywords: Scandium; Critical Zone; Laterite; Weathering; Mass-balance calculations; X-ray absorption.

1. Introduction

Knowledge of the geochemical behaviour of scandium (Sc) is limited, as substantial accumulations are scarce on Earth. Although Sc has a crustal abundance of *ca* 22 ppm (Rudnick and Gao, 2014), Sc-rich minerals are rare. Only a dozen mineral species are identified in Earth materials (Samson and Chassé, 2016). The 3*d* outer electronic configuration of Sc, shared with other first-row transition elements, its lithophile behaviour and low electronegativity and its single oxidation state (Sc^{3+}) in terrestrial redox conditions lead to its participation in solid solutions of rock-forming oxycompounds at low concentrations (Christy, 2015). This limits the formation of Sc mineral species and hinders preferential partitioning of Sc during most geochemical processes. With yttrium and the lanthanides, Sc belongs to

*Corresponding author.
Email address: mathieu.chasse@normalesup.org (Mathieu Chassé)

the rare-earth elements (REE) group (Connelly et al., 2005). Elements from this group share similar chemical properties, such as a trivalent oxidation state, rare processes that result in concentration and occurrence together in the same mineral deposits. In particular, major REE deposits are related to tropical weathering of carbonatite or granite (Verplanck, 2017) and Sc enrichment is common in laterites (Williams-Jones and Vasyukova, 2018). However, critical-zone (CZ, the interface between geological, hydrological and atmospheric compartments where rocks interact with air, water and biota) studies indicate differences between REE and Sc behaviour. In the regolith, REE are mobilised and redistributed through weathering processes (*e.g.* Braun et al., 1993, 1998; Chapela Lara et al., 2018). In contrast, in a variety of environments, ranging from bogs (Steinmann and Shotyk, 1997) to moderately weathered igneous rocks (Cramer and Nesbitt, 1983; Middelburg et al., 1988) and intensively weathered material (Schütz and Rahn, 1982; Nesbitt and Markovics, 1997; Brown et al., 2003), Sc is considered to behave as a conservative (*i.e.* relatively immobile) element, much like Ti, Zr or Nb. Scandium has thus been adopted as a conservative element to model accumulation or depletion processes in CZ studies (*e.g.* Shotyk et al., 2001; Eshel et al., 2015; Zhao and Zheng, 2015).

The CZ plays an essential role in ecosystems and predicting its response to anthropogenic forcing is a major challenge to preserve a sustainable environment (Goddéris and Brantley, 2013). A first step would be to model past long-term changes arising from natural processes (Brantley et al., 2016). Such information is recorded in the regolith but requires a careful interpretation of its geochemistry. In particular, mass-balance calculations are used to estimate mass fluxes and understand what controls the rates of regolith formation and transport (Brantley and Lebedeva, 2011). These calculations are based on the use of conservative elements, assumed to be immobile during weathering. This assumption is based on the low solubility of these elements and on the resistance to weathering of primary host minerals. However, there is evidence for mobilisation and redistribution of conservative elements which can be leached from or accumulate in specific horizons of the CZ (*e.g.* Cornu et al., 1999; Du et al., 2012; Schindler and Hochella, 2016). The mechanisms of element sequestration must be clarified to properly select the conditions in which they can be considered as immobile. As with other conservative tracers, Sc solubility in water is low. For instance, at near neutral pH and room temperature, Sc complexation by hydroxides results in a solubility below 10^{-6} mol $\cdot$ L^{-1} (Wood and Samson, 2006). However, Sc does not occur in minerals stable during weathering but is dispersed among major phases subject to weathering, raising questions about the processes controlling mobility and concentration of Sc in the CZ.

Scandium commonly concentrates in lateritic regoliths developed over mafic–ultramafic rocks. Concentrations reported in Australia, New Caledonia, the Caribbean, the Philippines, China, Ivory Coast and Guinea, reach 100 ppm in the Fe oxyhydroxide-rich horizons developed over peridotites (Jaireth et al., 2014; Aiglsperger et al., 2016; Maulana et al., 2016; Sun et al., 2017; Teitler et al., 2019). In eastern Australia, exceptional concentrations, reaching 800 ppm (Chassé et al., 2017) have been recognised over mafic–ultramafic intrusions (Fig. 1). Laterites are a major component of the CZ. These regoliths result from intense subaerial weathering of rocks in tropical environments, forming alteration layers frequently reaching several tens of meters in thickness. Laterites occur over 30 % of the Earth continents and represent 80 % of the volume of the soil mantle, thus having a major influence on the geochemical budget of weathering (Nahon, 2003). Like other regoliths, laterites result from the transfer of chemical elements between the different horizons of the CZ. However, the conditions in which laterites form are an extreme case of rock weathering. Elevated temperatures increase the kinetics of chemical reactions while intense rainfall repeatedly renews leaching waters, shifting chemical equilibria towards mineral dissolution (Tardy, 1993). Due to the intensity of these processes, lateritic samples give the clearest evidence of element mobilisation during oxidative weathering. Lateritic profiles also reveal the different steps of weathering, from the early breakdown of primary minerals to the induration of an oxide-rich lateritic cover (Anand and Paine, 2002). Finally, the preservation of lateritic profiles results from slow physical erosion. The timescales considered can reach tens of millions of years (Shuster et al., 2005) and reflect paleoclimatic events (Balan et al., 2005). In particular, eastern Australia is known for intense lateritisation since the middle Miocene (Metzger and Retallack, 2010). From that perspective, east Australian laterites constitute a unique opportunity to understand the processes affecting Sc dynamics in the CZ.

Despite the recent interest surrounding Sc in lateritic contexts, few data have been published that address the processes of concentration. In the weak and moderate stages of weathering, which result in the formation of saprolitic horizons at the expense of the parent rock, evolution of Sc speciation is unexplored. In-

formation on Sc speciation is limited to the lateritic duricrust and remains debated. Iron oxides and oxyhydroxides, known to play a critical role in binding trace elements via adsorption and structural incorporation (*e.g.* Brown et al., 1999; Cornell and Schwertmann, 2003; Frierdich et al., 2011), are ubiquitous in this horizon. Scandium correlation with Fe in weathered materials has long been established (*e.g.* Norman and Haskin, 1968; Das et al., 1971; Birgül, 1981), but the reasons for such an association remains unclear. Recent work has shown that Sc speciation in lateritic duricrust is dominated by adsorption on goethite while substitution is minor (Chassé et al., 2017), although Ulrich et al. (2019) suggest that Sc could be incorporated into the goethite structure (Ulrich et al., 2019). In addition, conservative behaviour of Sc is at odds with evidence of depletion at the top of lateritic duricrusts (Campodonico et al., 2019; Teitler et al., 2019). Atomic-scale processes at the interface between minerals and aqueous solutions exert a major control on the fate of metals in soils and sediments (Brown and Calas, 2012). The low metal concentrations often encountered in the CZ can limit the use of element specific structural tools such as X-ray absorption spectroscopy. The exceptional Sc concentrations found in east Australian laterites provide an opportunity to utilise mineralogical and spectroscopic techniques to determine the mechanisms governing the dynamics of this trace metal in the CZ. Through a multiscale approach, we analyse Sc dynamics in profiles from the Syerston–Flemington (New South Wales, Australia) laterite, developed over a mafic–ultramafic intrusion. We use geochemical calculations based on isocon analyses, revealing the horizons where Sc is sequestered or leached. Combining micron-scale techniques, including electron probe microanalysis (EPMA) and laser-ablation–inductively coupled plasma mass spectrometry (LA–ICPMS), with molecular-scale analyses using X-ray absorption near-edge structure (XANES) spectroscopy, we discuss the evolution of Sc speciation along a lateritic profile. We show the major role of clay minerals and environmental conditions in Sc immobilisation during early weathering stages. In the more intensely weathered lower lateritic duricrust, Sc mobility remains limited due to adsorption on Fe oxyhydroxides. In the upper horizons of lateritic profiles, dissolution–precipitation reactions of Fe oxides and oxyhydroxides drive Sc dynamics, with a downward migration favouring Sc concentration in the Fe oxyhydroxide-rich middle-part of the profiles.

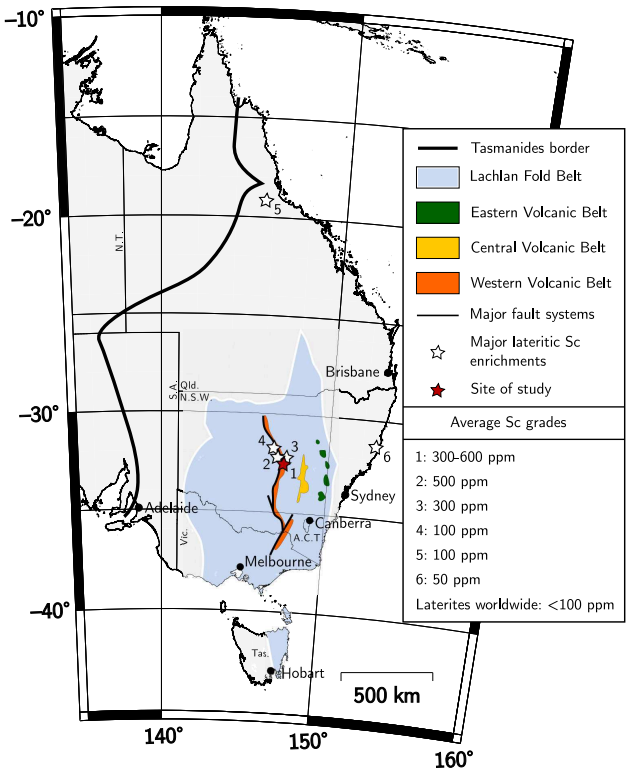

Figure 1: Location and geological context of the major lateritic Sc occurrences found in eastern Australia (1: Syerston–Flemington, site of study, 2: Hylea, 3: Owendale, 4: Nyngan, 5: Sconi, 6: Pacific Express). Scandium contents are given according to Byrne (2017); Gordon (2018); Moller et al. (2017); Ricketts and Duyvesteyn (2018); Bell (2018) and Durack (2018), respectively.

2. Material and Methods

2.1. Geological Context, Drill Core Description and Sampling

Aeromagnetic surveys and air-core drilling campaigns indicate that the studied lateritic cover (> 30 m thick) is developed above the Tout Intrusive Complex. This mafic–ultramafic complex is part of the Western Volcanic Belt (Fig. 1), a remnant of the Macquarie Arc, a supra-subduction zone system accreted during the Benambran Orogeny (*ca* 450 Ma, Crawford et al., 2007). The Tout Intrusive Complex, described as an Alaskan-type ultramafic complex, formed in a post-collisional, extensional setting dated at *ca* 440 Ma (Webb, 2014).
Two diamond-drill cores (JSD–001 and JSD–002) exhibiting horizons typical of this lateritic cover and zones with Sc enrichment were described (see Table EA1 for the location and detailed core logging, after Chassé et al., 2017). They comprise eight major horizons (Fig. 2a). The bottom saprock–saprolite horizon is more than 10 m thick. Although the drillings did not reach

unweathered bedrock, this horizon indicates that the parent rock is a clinopyroxenite. (ii) In rare levels, a serpentinised dunitic saprolite horizon was identified in contact with the saprolitic pyroxenite. These rocks are two of the lithotypes that compose the Tout Intrusive Complex underlying the lateritic cover (Andrew et al., 1995). (iii) The overlying plasmic zone, around 1 m thick, is dominated by a green clay phase. (iv) A mottled zone, about 3 m thick, is found above, dominated by a red–brown fine-grained matrix mixture of Fe oxides and oxyhydroxides with a clay mineral. Common clumps of green clay become accessory in the upper parts of this horizons. Two types of veins occur, black fine-grained veins of Mn oxides and white veins of calcite. (v) The complete dissolution of smectite and the relative enrichment in Fe oxides and oxyhydroxides characterises the main zone of the lateritic duricrust, a few meters to 10 m thick. (vi) The formation of a consolidated lateritic duricrust (*cuirasse*) about 5 m thick is limited and the induration by aggregation of the pisoliths in an Fe (oxyhydr)oxide-rich matrix is never complete. They are associated with a matrix of Fe oxides and oxyhydroxides and clay minerals. (vii) This vertical evolution seems to be disrupted around the top 10 m by allochtonous lateral input, identified from clasts and rare evidence of former alluvial channels, forming a mixed transported and residual lateritic duricrust. (viii) In the uppermost part of the profile, a lateritic gravel, less than a few metres thick, results from the collapse of the lateritic duricrust on contact with meteoric water and surficial biological activity. It consists of a mixture of pisoliths with residual lateritic material and soil.

From each diamond-drill core, 60 samples were collected (Table EA1), approximately every 50 cm. They were selected to be representative of each individual horizon, to sample veins or unusual textures inside a horizon, or to sample textural changes immediately below or above the different horizons. All bulk samples were studied using the mineralogical and chemical analyses procedures described below. Based on mineralogical and chemical results, 15 representative chip samples (Table EA1) were selected from each core for the subsequent analyses.

2.2. Mineralogical Analysis Procedures

The mineralogical composition of bulk powder samples was determined by XRD. The data were collected in Bragg-Brentano geometry with a PANalytical X'Pert PRO MPD diffractometer equipped with an X'Celerator detector. Cobalt Kα radiation ($\lambda_{K\alpha 1}$ = 1.78897 Å, $\lambda_{K\alpha 2}$ = 1.79285 Å) was used in order to minimise the effect of Fe fluorescence on background. Data were recorded over the 3 ° 2θ to 90 ° 2θ range, with 0.017 ° 2θ steps and a total counting time of 6 hours. Actinolite, anatase, andradite, boehmite, calcite, diopside, dolomite, gibbsite, goethite, hematite, kaolinite polymorphs, lithiophorite, magnetite/maghemite, opal–CT, quartz, smectite, todorokite and vermiculite were identified using International Centre for Diffraction Data (ICDD) references (PDF-2 database).

Least squares refinement of the XRD patterns obtained on laterite samples was performed using the Rietveld method, fitting the experimental patterns with theoretical ones calculated from the crystal structure of each phase identified in the sample. These refinements were carried out with the FullProf suite of programs (Rodríguez-Carvajal, 1993). Unit cell parameters, atomic positions, and isotropic Debye–Waller factors were refined from crystal structures obtained from the Crystallography Open Database. Mineral proportions were estimated from those refinements (Fig. EA1 and Table EA2).

2.3. Chemical Analysis Procedures

Chemical analyses have been carried out at the Geochemical Analysis Unit (GAU) of CCFS–GEMOC in the Department of Earth & Planetary Sciences at Macquarie University. Bulk chip samples from selected levels were powdered using a tungsten carbide mill to obtain a fine powder (below 50 μm in size). Care was taken when cleaning the mill with ethanol and Milli-Q® water between samples to avoid cross-contamination.

Standard X-ray fluorescence (XRF) techniques were used for major- and minor-elements analyses of bulk samples. One gram of powder of each sample was mixed with 10 g of lithium tetraborate-meta-borate (12:22 mixture) flux, fused in a platinum crucible and cooled to give glass discs. The discs were analysed using a PANalytical Axios 1 kW energy-dispersive XRF spectrometer. Loss on ignition was determined for each sample at 1100 °C overnight. The deviations from reference values from GeoReM (Jochum and Nohl, 2008) for standards BCR-2, BIR-1 and BHVO-2 have been used to estimate the instrumental error. Replicas of the samples have been used to estimate the sampling error. Analyses of the samples and reference materials can be found in Tables EA3 and EA4.

Concentrations of Sc and other trace elements were determined in the bulk samples by standard ICP–MS methods. Hundred milligrams of sample powder were weighed into clean Savillex® Teflon beakers. Samples were then digested following the steps below:

1. Digestion in a 1:1 mixture of HF (Merck, Suprapur

grade) and HNO_3 (Merck, AR grade, Teflon distilled) for 24 h at 160 °C followed by evaporation to dryness at 150 °C.
2. Digestion in a 1:1 mixture of HF and perchloric acid ($HClO_4$, Merck, Suprapur grade) for 3 days at 170 °C followed by evaporation to dryness at 120 °C, 150 °C and then 170 °C.
3. Digestion in a 1:1:1 mixture of HF, HCl (Merck, AR grade, Teflon distilled) and $HClO_4$ for 3 days at 170 °C followed by evaporation to dryness at 170 °C to 190 °C.
4. Digestion in aqua regia (HNO_3 + 3HCl) for 3 days at 150 °C followed by evaporation to dryness at 150 °C.
5. Digestion in 6N HCl solution for 12 h at 150 °C followed by evaporation to dryness at 150 °C.
6. Digestion in 6N HNO_3 for 12 h at 150 °C followed by evaporation at 120 °C.

Samples were then diluted to 100 mL in a 2 % HNO_3 and 0.25 % HF solution. These 1:1000 dilutions were individually spiked with a 15 μL aliquot of a solution of ^{6}Li, As, Rh, In, Tm and Bi in 2 % HNO_3. The samples and standards were analysed using a quadrupole Agilent 7500c/s ICP–MS. The BCR-2 reference basalt was used as a calibration standard to correct for instrument sensitivity. Run drift was corrected using the aliquot of solution added to each sample. Background was measured on a 2 % HNO_3 rinse solution. The deviations from reference values from GeoReM (Jochum and Nohl, 2008) for standards BCR-2, BIR-1 and BHVO-2 have been used to estimate the instrumental error. Duplicates of the samples have been used to estimate the sampling error. Analyses of the samples and reference materials are given in Tables EA3 and EA4.

2.4. Isocon Analysis Procedures

The isocon method (Grant, 1986) has been applied to evaluate element redistribution through the lateritic profiles using the results obtained from chemical analyses. Results are given in Table EA5. The method is based on a choice of elements considered as immobile during alteration to determine the variations in the concentrations of other elements in altered samples relative to the concentrations in the parent rock. The composition of the unaltered parent rock has been chosen based on mineralogical and geochemical considerations. Even the deepest levels of each profile are slightly altered. However, in the saprock several samples contain only traces of clay phases, indicating weak alteration. Among these samples, those containing detectable andradite or actinolite were considered as unrepresentative of the parent rock and removed. Most of the samples from the saprock do not contain detectable levels of these minerals. From the remaining samples, those richest in Mg and Ca and poorest in Fe have been selected as the closest to the parent rock, considering that Mg and Ca are the first elements to be leached while Fe is immobile during early stages of alteration of clinopyroxenes. Samples JSD1–240 and JSD2–310 were selected as typical parent rock for the JSD–001 and JSD–002 profiles, respectively.

The choice of immobile elements, Ti, Zr and Nb, was made combining geochemical considerations and analyses of isocon diagrams, giving the concentration of the elements considered in the altered sample versus their concentration in the parent rock. In such diagrams, ideally immobile elements will form a line, called an isocon, passing through the origin. Representative isocon diagrams are presented for the main horizons of each lateritic profile (Fig. EA2) showing that Ti, Zr, Nb and Hf can be considered as immobile in our profile. The isocon line is located above elements leached during lateritic alteration such as Li, Mg or Ca and below elements known to accumulate in specific horizons, such as Mn in the mottled zone or Ni in the saprolite and plasmic zone. Whatever the combination of immobile elements selected, no significant difference is observed in the variation of Sc concentration relative to the parent-rock concentration along the profiles (Fig. EA3). The isocon method allows averaging of the error made when selecting one element at the expense of another. Considering Ti, Zr and Hf together could create a bias in the analyses. The close chemical properties of these three elements (IVB family of the periodic table) make them likely to be mobilised together for a given geochemical process. It is also of interest to use elements within a large range of different concentrations to limit the influence of geochemical processes that may affect the mobility of individual elements differently depending on their concentration. Titanium, Zr and Nb, often used for mass-balance calculations exploring lateritic weathering (Aiglsperger et al., 2016), were thus selected.

2.5. Sequential Extraction Procedures

A sequential extraction of the different fractions of bulk powder samples has been carried out (Hall et al., 1996). Approximately 1 g of sample powder was weighed into a 50 mL centrifuge tube. The adsorbed and exchangeable fractions were extracted using 20 mL of 1.0 mol $\cdot$ L^{-1} CH_3COONa at pH 5, added to the powder sample, capped, vortexed for 10 s and placed in a horizontal shaker for 6 h. The suspension was centrifuged for 10 min at 5000 rpm and the supernatant liquid was decanted and placed in a labelled test tube. The

residue was then rinsed with 5 mL of Milli-Q® water, vortexed for 10 s and centrifuged again 10 min at 5000 rpm. The operation was repeated twice and the supernatant was added to the test tube. These steps were repeated for a second leaching of the residue. The amorphous iron oxide fraction was extracted using 20 mL of 0.25 mol $\cdot$ L^{-1} $NH_2OH \cdot HCl$ in 0.25 mol $\cdot$ L^{-1} HCl added to the residue obtained after extraction of the adsorbed and exchangeable fraction. The centrifuge tube was capped, vortexed for 10 s and placed in a water bath at 60 °C for 2 h with the cap loosened. Every 30 min, the centrifuge tube was closed and vortexed. The suspension was centrifuged for 10 min at 5000 rpm and the supernatant liquid was decanted and placed into a new labelled test tube. The residue was then rinsed with 5 mL of Milli-Q® water, vortexed for 10 s and centrifuged again 10 min at 5000 rpm. The operation was repeated twice and the supernatant was added to the test tube. These steps were repeated for a second leaching of the residue with only 30 min in the water bath. Scandium concentrations were measured by ICP–MS, following the procedure described above. Analyses of the samples and reference materials are given in Table EA6, the composition of the residue was deduced from whole-rock analyses.

2.6. Adsorption Experiment Procedures

Experimental adsorption of Sc was performed on pure synthetic goethite and hematite. Details on the synthesis protocol are given by Chassé et al. (2017). Scandium chloride hexahydrate was diluted in water to obtain $ScCl_3$ solutions at 10 ppm, 20 ppm, 50 ppm, 100 ppm, 200 ppm, 500 ppm and 1000 ppm Sc. Scandium adsorption has been carried out by adding 10 mL of $ScCl_3$ solution to 1 g of goethite or hematite. The solid and the solution were shaken together for 24 h. The measured pH was *ca* 6. The solid was then separated by centrifugation and dried at 45 °C for 24 h. Scandium concentrations in the solution and solid residue were measured by ICP–MS, following the procedure described above. Analyses of the solid and solutions are given in Table EA7.

2.7. Spatially-Resolved Chemical Analyses

Polished sections of selected samples were made by impregnating dry chips in polyester resin diluted with acetone and polishing on cloth with diamond pastes.
Scanning electron microscope (SEM) analyses were carried out using a field emission SEM (FEG–SEM Zeiss SUPRA 55VP). A Bruker QUANTAX EDS system including a QUAD silicon drift detector (SDD) was used for energy dispersive X-ray spectrometry (EDXS). Electron probe microanalyses were performed to obtain major- and minor-element concentrations on selected phases along with chemical mapping of polished sections using a Cameca SXFive EPMA equipped with five wavelength-dispersive spectrometers (WDS) at the Centre d'analyse des minéraux de Paris (CAMPARIS, Sorbonne Université). Each point was probed with a focused 20 kV, 40 nA beam for major elements and with a focused 20 kV, 200 nA beam for minor and trace elements. Major elements (Na, Mg, Al, Si, P, Cl, K, Ca, Ti, Cr, Mn, Fe and Ba) were analysed with a 20 s (peak + background) counting time. Scandium was analysed with 60 s (peak + background) counting time. The WDS used the following monochromators: a large area (1320 mm^2) thallium acid pthalate (TAP) to collect Na, Mg and P Kα X-rays; a regular (660 mm^2) TAP to collect K and Ca Kα X-rays; a regular (660 mm^2) pentaerythritol (PET) and two large (1320 mm^2) lithium fluoride (LiF) to collect Cr, Mn, Fe, Ti and Sc Kα X-rays. The two large LiF monochromators were used simultaneously to analyse each of the minor and trace elements. Detection limits as low as 60 ppm to 30 ppm were achieved with this method. Wavelength-dispersive spectrometer analyses were performed using the following standards: albite for Na; diopside ($CaMgSi_2O_6$) for Mg, Si and Ca; apatite Durango for P; orthoclase ($KAlSi_3O_8$) for Al and K; Cr_2O_3 for Cr; $MnTiO_3$ for Mn and Ti; hematite for Fe and Sc_2O_3 for Sc.
Laser-ablation ICP–MS has been used to analyse the scandium composition on selected areas of the polished sections at the Geochemical Analysis Unit (GAU) of CCFS–GEMOC in the Department of Earth & Planetary Sciences at Macquarie University. The use of EPMA to measure Sc content was precluded in the saprolite due to high Ca content inducing X-ray lines overlap with Sc. Analyses were performed using a Photon Machine Excite 193 nm ArF Excimer laser attached to an Agilent 7700 ICP–MS system. Beam size ranged between 10 μm and 60 μm at a pulse rate of 5 Hz and an energy density of 3.0 J $\cdot$ cm^{-2} to 4.4 J $\cdot$ cm^{-2}. Each analytical sequence started with 60 s of background, 120 s during ablation and 30 s of washout. NIST SRM610 was used as an external standard and ^{43}Ca was taken as the internal standard for clinopyroxene, Ca-bearing silicate clays and apatite, ^{27}Al was used for Al-bearing Fe oxides and oxyhydroxides and Al oxyhydroxides, ^{29}Si was used for Ca-poor silicate clays, quartz and amorphous silica and ^{57}Fe was used for Al-poor Fe oxides and oxyhydroxides. The data reduction software GLITTER 4.4 (Griffin et al., 2008) was used to calibrate the fractionation induced by ablation, transportation and excita-

tion processes. Standards BCR-2G and NIST SRM610 were included as unknown samples in each batch for quality control. The in-house chromite standard LCR-1 was used to check the quality of the measurements for Fe-rich samples.

2.8. Synchrotron-Based Analysis Procedures

X-ray absorption data were collected on the LUCIA beamline (Vantelon et al., 2016) at the SOLEIL synchrotron in Paris and on the ID21 beamline (Salomé et al., 2013) at the European Synchrotron Radiation Facility (ESRF) in Grenoble. The former operated with a storage ring current of 450 mA and an energy of 2.75 GeV while the latter operated with a storage ring current of 200 mA and an energy of 6 GeV.

XANES spectra were collected using an Si(311) and an Si(220) double crystal monochromator on LUCIA and ID21, respectively. The monochromators were calibrated against the maximum intensity of the first inflection of the first derivative of a Sc_2O_3 standard (4492.8 eV) for XANES measurements at the Sc *K*-edge. Scandium *K*-edge XANES measurements were performed in the energy range 4400 eV to 4800 eV. The energy step at the Sc *K*-edge was (5, 0.2, 0.5 and 1) eV for energy ranges of (4400 to 4485) eV, (4485 to 4534) eV, (4534 to 4586) eV and (4586 to 4800) eV, respectively. Spectra were collected at room temperature, under vacuum. The spectra were collected in XRF mode on pellets obtained from powdered material and mounted on a holder between two Ultralene® films, using a four-element SDD. Several spectra were acquired for each sample to reduce the noise; individual spectra acquired on each spot were merged to obtain average spectra before background subtraction and normalisation using the PyMCA software (Solé et al., 2007). No spectra could be recorded in the saprock due to the high X-ray fluorescence of Ca in these samples, combined with the lowest Sc contents observed in the profile, hiding the XANES signal of Sc.

In order to analyse the results obtained on natural samples, we obtained various Sc-bearing phases to be used as references for comparison. Details of Sc-adsorbed and Sc-substituted goethite and hematite are given in Chassé et al. (2017). Scandium-adsorbed smectite has been obtained by adding 10 mL of $ScCl_3$ solution at 1000 ppm Sc to 1 g of pure natural montmorillonite commercialised by Sigma–Aldrich. The solid and the solution were shaken together for 24 h. The solid was then separated by centrifugation and dried at 45 °C for 24 h. For comparison with Sc-adsorbed smectite, an Sc-substituted smectite was obtained from a smectite-rich sample, containing only minor hematite and goethite, as deduced from XRD. The Fe oxide and oxyhydroxide fraction has been removed from this sample following the dithionite–citrate–bicarbonate (DCB) treatment (Mehra and Jackson, 1958). About 8 g of sample was placed in a 100 mL centrifuge tube and 80 mL of 0.3 mol $\cdot$ L^{-1} trisodium citrate ($Na_3C_6H_5O_7$) and 10 mL of 1 mol $\cdot$ L^{-1} $NaHCO_3$ was added. The solution was heated at 80 °C in a water bath with one gram of solid Na_2SO_4. The sample was stirred for 1 min and then occasionally shaken over a period of 60 min. The suspension was then centrifuged at 5000 rpm and the supernatant liquid was decanted. The operation was repeated until the supernatant was clear. A final washing was made with the trisodium citrate solution. The remaining Sc was shown to be substituted in smectite as its XANES spectral signature is distinct from that of Sc-adsorbed smectite.

3. Results

3.1. Mineralogical and Geochemical Evolution of the Lateritic Profiles

Rietveld refinement of XRD patterns indicate that the saprock–saprolite horizon is dominated by diopside, a clinopyroxene, constituting more than 90 wt% of the samples on average (Fig. 2b). Minor smectite and hematite are also observed in this horizon. Some levels exhibit low (up to 10 wt%) proportions of andradite, a garnet. Opal–CT is dominant in the dunitic saprolite, associated with minor hematite and maghemite. The plasmic zone is characterised by the complete disappearance of diopside and the dominance of smectite, associated with newly formed minor Fe oxides and oxyhydroxides: goethite, hematite and maghemite. Quartz and carbonates are present in veins. The mottled zone is marked by the disappearance of smectite, replaced by kaolinite, while hematite and goethite contents continue to increase and minor Mn oxides are found. The main zone of the lateritic duricrust is composed of an assemblage of kaolinite, goethite and hematite with minor maghemite and anatase. The *cuirasse* horizon is characterised by the replacement of kaolinite by gibbsite. Mineralogical differences between the transported–residual lateritic horizon and the lateritic duricrust are limited but the reappearance of kaolinite and the increasing quartz and dolomite proportion is associated with the presence of detrital materials. The lateritic gravel at the top of the profile is characterised by significant proportions of quartz. This level is also characterised by the presence of boehmite.

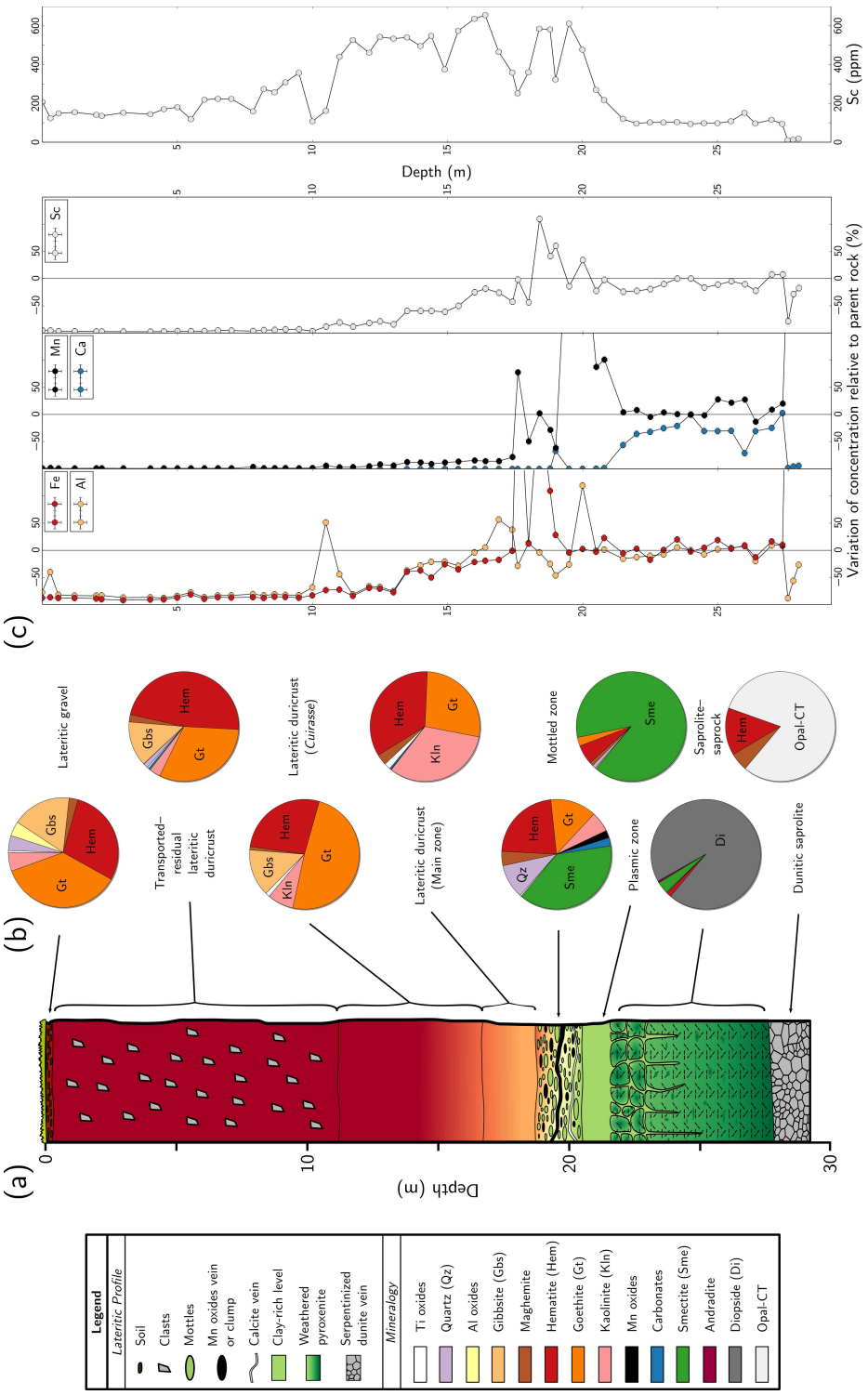

Figure 2: Mineralogical and geochemical evolution of a typical Sc-rich lateritic profile from the Syerston–Flemington deposit. (a) Diagram representing the different horizons identified in a typical profile. (b) Pie charts presenting the average proportion of each mineral phase identified by X-ray diffraction in a given horizon. Mineral proportions in the main zone and *cuirasse* of the lateritic duricrust are from Chassé et al. (2017). (c) Variations of the concentrations of selected elements (Fe, Al, Mn, Ca and Sc) relative to their parent-rock concentrations along the profile determined using the isocon method. The evolution of Sc concentration along the profile is after Chassé et al. (2017).

The geochemical evolution of the profile was analysed through mass-balance calculations using the isocon method indicating gains or loss of mass relative to Ti, Zr and Nb (Fig. 2c). In parallel, absolute Sc concentrations are given. The dunite saprolite has low Sc contents (*ca* 10 ppm to 20 ppm). From the clinopyroxenite saprock to the plasmic zone, Sc concentration increases from *ca* 85 ppm to 300 ppm. Mass-balance results indicate an intense leaching of major mobile ions such as Ca^{2+} and Mg^{2+} while there is no relative gain or loss of Sc. Carbonate- and quartz-rich zones in the saprolite and plasmic zone are associated with relative loss of Sc and low Sc concentrations. Sc concentration continues to increase in the mottled zone while relative Sc gains are observed. The mottled zone is also associated with the redistribution and relative mass gain in specific elements, depending on the mottle under study. In the lateritic duricrust, Sc concentrations are the highest but mass loss is observed to a lesser extent than major elements. An increase in mass loss is observed at the transition between the residual lateritic duricrust and the transported one.

3.2. Scandium Content in Identified Mineral Phases

In the saprock, SEM–EDXS mapping confirms the dominance of clinopyroxene (Fig. 3) which chemical composition obtained by EPMA analysis corresponds to diopside (Table 1). In rock fractures, apatite and andradite can be identified chemically. Preserved relicts of a layered mineral, petrographically identified as biotite but from which K is absent, has a composition corresponding to vermiculite. Inclusions of Fe oxides in clinopyroxenes have significant Cr contents, suggesting that they represent primary oxides. A clay phase, present at the border of clinopyroxene grains, has the composition of ferrosaponite, a smectite. Despite systematic SEM–EDXS mapping, no discrete Sc phases could be found. Among primary or hydrothermal phases, LA–ICPMS indicate that only two have significant Sc contents: diopside (*ca* 80 ppm) and andradite (*ca* 250 ppm). Smectite, resulting from supergene weathering, also contain high Sc concentrations (*ca* 130 ppm).

In the saprolite and plasmic zone, textural imaging and chemical mapping performed using SEM indicate that the matrix of the polished sections is dominated by Si, Fe, Al and Mg, with variable contents in Fe (Fig. 4). Averaged EPMA compositions on representative spots (Table 1) indicate that this matrix has a composition similar to ferrosaponite with excess Fe, indicating the presence of fine-grained Fe oxyhydroxides and explaining the brownish colour of the polished sections. Layered pseudomorphs are remnants of biotite, with the composition of vermiculite. Two types of Fe oxides can be distinguished from their Cr content. Systematic SEM–EDXS mapping found no newly formed discrete Sc phases. The mixture of smectite and Fe (oxyhydr)oxides contains *ca* 300 ppm Sc on average. Vermiculite replacing biotite is poorer in Sc than the matrix. Iron-oxide grains with significant Cr contents (Fe ox. 1) are the lowest in Sc (*ca* 20 ppm) while Fe-oxide grains with low Cr contents have higher Sc content (*ca* 70 ppm).

In the lateritic duricrust, SEM–EDXS mapping and EPMA compositions of identified phases are reported by Chassé et al. (2017). Scandium contents in kaolinite, quartz, gibbsite or anatase are low and no discrete Sc phase is observable. Two types of Fe-rich grains can be identified : almost pure Fe oxides with some Ti and Cr and low Al and Fe-rich grains with significant amounts of Al and low analytical totals, indicating a hydrated mineral (Table 1). Considering the mineralogical composition deduced from XRD and the abundance of these grains, they can only be attributed to hematite for the former type of grain, and Al-bearing goethite for the latter. Iron-oxide grains, carrying most of the Sc are not homogeneous in the studied samples, zoning and replacement of one Fe-rich phase by another is often found (Fig. 5). Zoned goethite grains (Fig. 5a) show that increasing Al content is associated with increasing Sc concentrations. Replacement of the rims of goethite grains by hematite (Fig. 5b) leads to a drastic drop in Sc concentration.

3.3. Scandium Speciation Determined by XANES Spectroscopy and Selective Leaching

Average Sc speciation has been studied using XANES spectroscopy at the Sc *K*-edge on powdered whole-rock samples (Fig. 6a, coloured spectra). The spectra on natural samples have been compared with those of potential Sc carriers for fingerprint analyses: goethite, hematite and smectite, with Sc either incorporated or adsorbed at the surface (Fig. 6b, black spectra). No spectra could be recorded in the saprock due to X-ray fluorescence resulting from high Ca contents. Significant changes in bulk Sc speciation from the plasmic zone to the lateritic duricrust are evidenced. In the plasmic zone, the spectra of the natural samples exhibit two main structures at *ca* 4512 eV and *ca* 4522 eV, distinct from the featureless spectra of Sc-adsorbed smectite or Fe oxide or oxyhydroxide. The relative intensity of the main features is inconsistent with the spectrum of Sc-substituted goethite and the shoulders observed beside the main features of the spectrum of Sc-

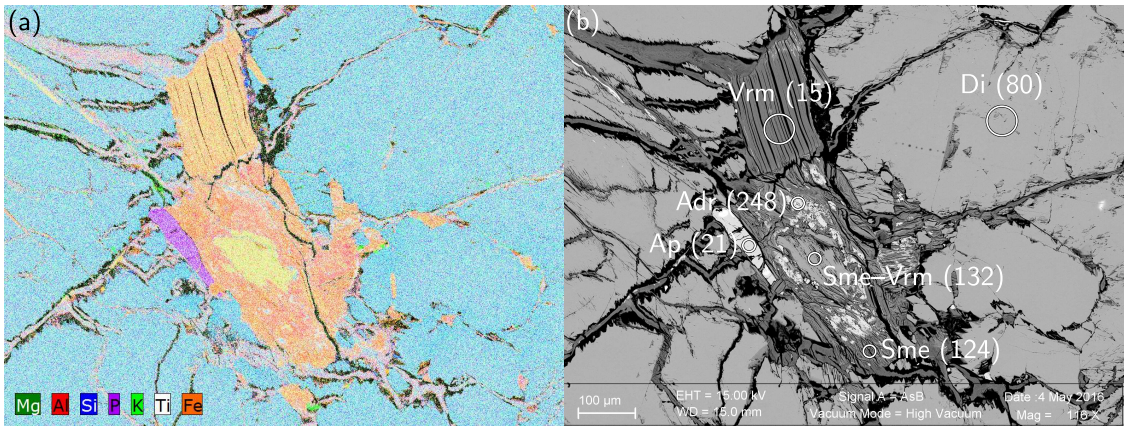

Figure 3: Characteristic textures and related Sc contents of the slightly altered parent clinopyroxenite (sampling depth: 29.2 m, JSD–002 core). (a) Scanning electron microscope (SEM)–energy dispersive X-ray (EDX) mapping showing the parent clinopyroxenes and focusing on an area exhibiting accessory minerals resulting from hydrothermal circulations in the protolith. (b) SEM image showing compositional contrast (angle selective backscattered electron detector) in the corresponding area. Scandium concentrations in ppm, measured by laser ablation–inductively coupled plasma mass spectrometry (LA–ICPMS), are given in parentheses along with the position of the ablation spot for each phase observed (Adr: andradite, Ap: apatite, Di: diopside, Sme: smectite, Vrm: vermiculite).

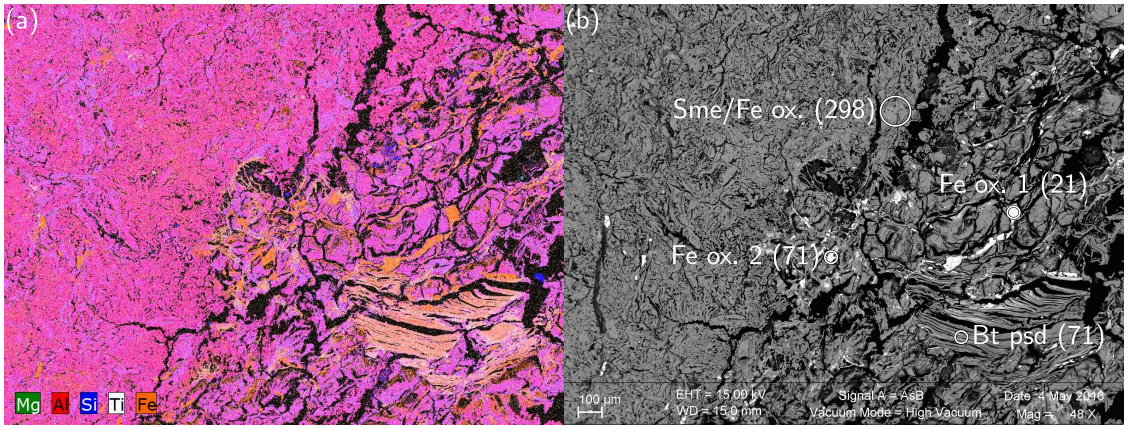

Figure 4: Characteristic textures and related Sc contents in the saprolite (sampling depth: 25.5 m, JSD–002 core). (a) SEM–EDX mapping showing major-element composition of a typical area of the plasmic zone distinguishing Fe oxides and oxyhydroxides from the matrix and evidencing a layered pseudomorph after biotite. (b) SEM image showing compositional contrast (angle selective backscattered electron detector) in the corresponding area; Sc concentrations in ppm, measured by LA–ICPMS, are given in parentheses beside the ablation spot for each phase (Bt: biotite, psd: pseudomorph, ox.: oxide, Sme: smectite).

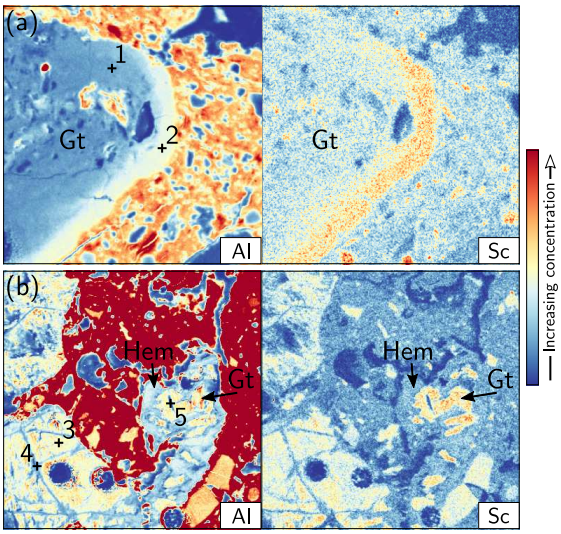

Figure 5: Electron microprobe mapping of Al and Sc contents in two grains from the lateritic duricrust (sampling depth: 12.5 m and 11.0 m, JSD–002 core): (a) goethite (Gt) grain exhibiting chemical zoning with increasing Al and Sc contents at the grain rim; (b) goethite grain exhibiting dissolution and replacement by hematite (Hem) at the rim, associated with drastic drop in Sc content. The numbers correspond to the chemical composition of the different areas of each grain given in Table 1.

substituted hematite are absent. By contrast, the spectra from the plasmic zone are identical to that of Sc substituted into the smectite structure. From the mottled zone to the top of the lateritic duricrust (Fig. 6a), Sc *K*-edge XANES spectra show broad features characteristic of Sc adsorbed on mineral surfaces. In samples from the transported lateritic duricrust, the shift of the edge crest from *ca* 4508 eV to *ca* 4511 eV indicates a minor contribution of substituted Sc in the hematite structure. Selective leaching experiments do not reveal significant differences in the proportion of Sc included in the different fractions, whatever the horizon considered (Fig. 6b) which indicates that the different leaching steps are inefficient in extracting Sc. Only a minor proportion of adsorbed Sc is exchangeable by this method or accessible to the leaching solutions (< *ca* 10 %).

3.4. Iron (Oxyhydr)oxides Capacities for Scandium Adsorption

Different adsorption capacities of goethite and hematite for Sc are evidenced by adsorption experiments (Fig. 7). At pH values representative of natural waters, only *ca* 10 % of Sc is adsorbed by hematite for Sc concentration in solution ranging from 10 ppm to 1000 ppm. The Sc adsorption rate at the surface of goethite decreases exponentially from *ca* 100 % to 10 % for Sc concentrations in solution ranging from 10 ppm to 1000 ppm.

3.5. Evolution of Trace-Element Patterns along the Lateritic Profiles

In order to compare the behaviour of Sc and other trace elements in the studied profiles, we followed the evolution of median trace-element patterns along the lateritic profiles (Fig. 8). From the saprolite to the top of the lateritic duricrust, elements considered as immobile during lateritic weathering, Ti, Zr and Nb, are consistently enriched. As noticed, Sc enrichment occurs up to the main zone of the lateritic duricrust. Scandium content stagnates in the *cuirasse* and decreases upwards. Enrichment of REE is at a maximum in the plasmic zone and decreases upwards. The negative cerium anomaly observed in the saprolite becomes positive upward in the profile.

4. Discussion

4.1. Evolution of Scandium Mobility and Carrier Phases along a Lateritic Profile

In the least altered saprock, the Sc content of clinopyroxene (*ca* 80 ppm Sc, Fig. 3) is comparable to whole-rock content (*ca* 85 ppm, Table EA3) demonstrating the importance of this phase in the overall Sc budget of the underlying clinopyroxenite parent rocks. The assemblage of andradite, apatite and biotite pseudomorphs in rock fractures indicates the occurrence of a secondary hydrothermal process. High Sc concentrations exhibited by andradite (*ca* 250 ppm) indicate the potential role of secondary hydrothermal alteration and metasomatism in redistributing part of the Sc within the Tout Intrusive Complex. The difference in Sc concentration between clinopyroxene and slightly altered whole-rock saprock samples, reaching *ca* 100 ppm (Table EA3), is explained by the presence of trace to minor smectite with high Sc concentrations (*ca* 130 ppm, Fig. 3), resulting from the weathering of clinopyroxene. Rare dunitic veins are reported to cross the host clinopyroxenite of the Tout Intrusive Complex (Andrew et al., 1995). This part of the saprolite is dominated by opal–CT, a phase found in the late stages of alteration of serpentinised dunites (Butt and Cluzel, 2013). The low Sc contents (*ca* 10 ppm–20 ppm, Table EA3) of the dunitic veins confirm that olivine and serpentinisation products are not efficient carriers of Sc (Samson and Chassé, 2016; Chassé et al., 2018a; Teitler et al., 2019).

In the saprolite and plasmic zone, recording the first stages of alteration of the clinopyroxenite and leading to

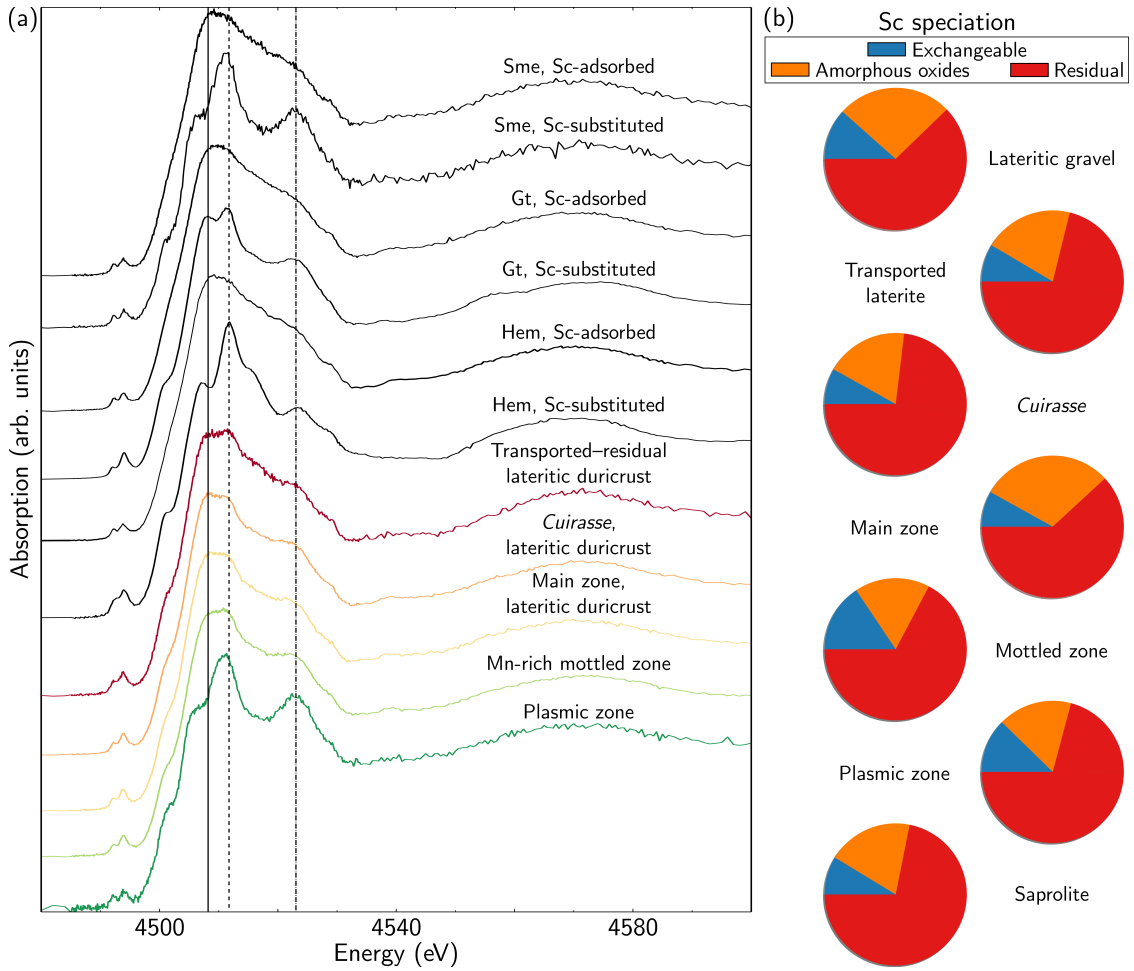

Figure 6: Evolution of Sc speciation with depth through a lateritic profile. (a) Evolution of whole-rock Sc *K*-edge XANES spectra in a lateritic profile (coloured spectra). The depth and core of origin of analysed samples is: 20.5 m, JSD–001 core (plasmic zone); 19.5 m, JSD–001 core (Mn-rich mottled zone); 18.0 m, JSD–002 core (main zone, lateritic duricrust); 13.5 m, JSD–001 core (*cuirasse*, lateritic duricrust); 6.5 m, JSD–001 core (transported–residual lateritic duricrust). The black spectra were recorded on synthetic powdered reference materials prepared with adsorbed or substituted Sc (gt: goethite, hem: hematite, sme: smectite). Spectra from Sc-bearing goethite and hematite are from Chassé et al. (2017). Spectra of adsorbed Sc are characterised by a single broad, featureless edge crest from *ca* 4508 eV to *ca* 4511.5 eV. Spectra of Sc-substituted goethite, hematite and smectite exhibit three main features at *ca* 4506 eV, *ca* 4511 eV and *ca* 4523 eV, but their relative intensity is distinct. Additional shoulders are visible at *ca* 4515 eV and *ca* 4528 eV on the spectrum of Sc-substituted hematite. (b) Pie charts presenting the average fraction of Sc recovered from selective leaching of each horizon identified in a typical lateritic profile.

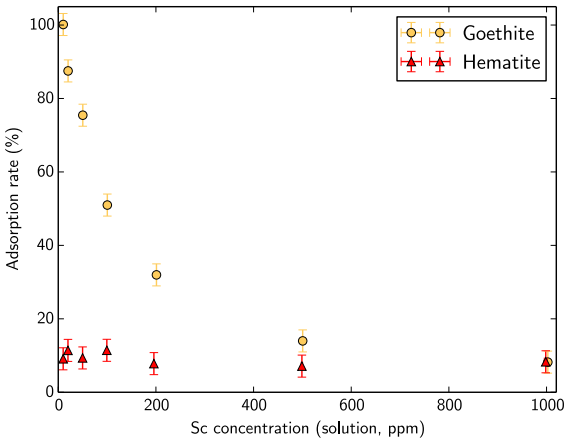

Figure 7: Scandium adsorption rates on goethite and hematite surfaces depending on Sc concentration (pH ≃ 6).

the formation of smectite and trace to minor Fe oxides and oxyhydroxides, Sc concentrations reach 300 ppm, and isocon analyses indicate that it is immobile (Fig. 2). Increasing Sc concentrations result from the process of relative enrichment that accompanies the leaching of mobile ions, such as Ca^{2+} and Mg^{2+}, while Sc is trapped by the newly formed minerals. In contrast, carbonate-rich zones in the saprolite and plasmic zone are associated with a loss of Sc from the initial stock, indicating that carbonates are not significant hosts to Sc (Tables EA3 and EA5). Most of the Sc budget is contained in the homogeneous matrix of smectite and Fe oxides and oxyhydroxides, with Sc contents (*ca* 300 ppm on average, Fig. 4) similar to that in the saprolite (from 300 ppm to 350 ppm, Fig. 2c). Two types of coarse Fe oxides are also present and distinguished by their Cr content (Fig. 4 and Table 1). The presence of Cr reflects their primary origin, while the absence of Cr indicates a later generation (Oze et al., 2004). Iron oxides of primary origin have the lowest Sc content (Fig. 4) as expected from the low initial content in these oxides from the parent rock (Table 1). Secondary Fe oxides, coarser than those found in the matrix but not mixed with smectite, are also low in Sc (*ca* 70 ppm, Fig. 4) indicating the low efficiency of these well-crystallised oxides in trapping Sc.

In the lateritic duricrust, Sc reaches its highest concentration (Fig. 2c). This enrichment results from the low mobility of Sc relative to major- and minor elements. Nonetheless, isocon analyses indicate mass loss relative to the initial stock available in the parent rock in the lateritic duricrust, while mass gains are observed in the mottled zone (Fig. 2c and Table EA3). This indicates that relative enrichment is associated with absolute enrichment through partial redistribution from upper horizons towards lower ones. The transition between the cuirasse and the transported lateritic duricrust, at a depth of *ca* 11 m (Fig. 2a), is marked by Sc loss reaching almost 100 % (Fig. 2c). The transported origin of this duricrust is evidenced by the increasing proportion of quartz and carbonates, reflecting a detrital origin (Fig. 2b and Table EA2). The isocon method estimates variations in concentrations relative to the parent rock. The drastic Sc depletion occurring at the exact depth of the observed transition with the transported lateritic duricrust (Fig. 2) suggests that the transported lateritic duricrust and the lateritic gravel above come from a parent rock distinct from the clinopyroxenite, with low Sc content. In these horizons, qualitative mineralogical differences cannot explain the evolution of Sc mobility. Varying proportions of kaolinite, quartz and gibbsite are observed (Fig. 2b), but they are poor Sc scavengers (Chassé et al., 2017). The role of lateritic Mn oxides in trapping Sc has been discussed by Audet (2008). However, they are largely absent in these horizons. The presence of significant proportions of lithiophorite in rare levels of the lateritic duricrust (Table EA2) is associated with low Sc contents compared to lower or upper horizons, and significant mass loss relative to the initial stock (Tables EA3 and EA5). These phases form after redistribution and concentration of Mn through circulating fluids (Post, 1999). At that stage, Sc is already trapped due to its low solubility (Wood and Samson, 2006) and is not available to be scavenged by Mn oxides. The different horizons are dominated by Fe oxides and oxyhydroxides, in the form of goethite and hematite (Fig. 2b and Table EA2). Ferric oxides thus control Sc dynamics in these horizons. Goethite is the main host for Sc in laterite (Chassé et al., 2017). A minor proportion of Sc is trapped by hematite. During the evolution of goethite grains, the progressive precipitation of Al-rich goethite rims surrounding earlier Al-poor goethite cores traps increasing Sc concentrations (Fig. 5a). In parallel, the replacement of the goethite rims by hematite leads to a drastic drop in Sc concentration (Fig. 5b), confirming the low affinity of hematite for Sc. This different affinity for goethite and hematite is supported by adsorption experiments showing that, at Sc concentrations and pH representative of natural waters, only 10 % of Sc is trapped by hematite while more than 90 % of Sc is adsorbed at goethite surface (Fig. 7). Scandium can be mobilised at the mineral scale during dissolution or reprecipitation of goethite and hematite.

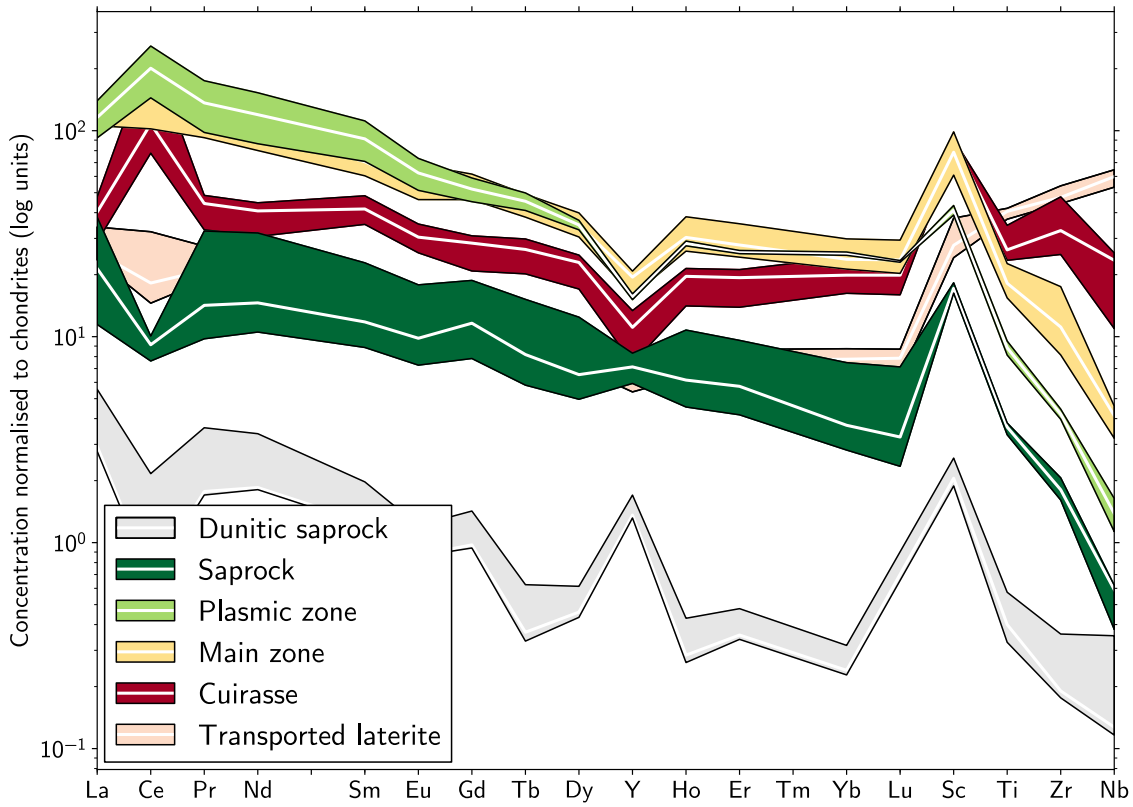

Figure 8: Evolution of trace-element patterns in the main horizons identified in a typical Sc-enriched lateritic profile. The white line marks the median pattern of the horizon. The range of each pattern is delimited by the first and third quartile pattern for each horizon.

Horizon	Saprock							Saprolite					Lateritic duricrust				
Phase/Grain	Di	Vrm	Ap	Adr	Fe ox.	Sme	Sme–Vrm	Alt. bt	Fe ox. 1	Fe ox. 2	Sme/Fe ox.		1 (Gt)	2 (Al-Gt)	3 (Al-Gt)	4 (Hem-rich)	5 (Hem)
N (EPMA)	7	5	2	1	2	4	2	3	7	7	10		3	2	4	3	1
SiO_2 (wt%)	53.2	38.3	0.4	33.7	0.7	48.4	43.4	35.3	1.5	4.2	45.8		4.8	6.4	5.4	4.5	0.2
TiO_2 (wt%)	0.2	5.2	0.0	1.7	0.5	0.2	1.2	1.1	0.9	0.8	0.4		1.5	0.9	1.5	1.3	1.1
Al_2O_3 (wt%)	2.1	11.7	0.0	5.8	1.5	5.7	11.2	13.8	1.1	0.7	6.8		2.9	12.6	4.3	2.5	0.4
Fe_2O_3 (wt%)	5.4	7.7	0.3	19.3	90.5	13.5	9.3	6.9	83.9	84.1	20.1		77.4	50.8	70.4	79.9	94.3
Cr_2O_3 (wt%)	0.2	0.3	0.0	0.2	5.5	0.2	0.3	0.3	2.8	0.1	0.3		0.1	0.0	1.5	0.2	2.5
MnO (wt%)	0.1	0.0	0.0	0.1	0.3	0.2	0.0	0.0	0.1	0.3	0.0		1.9	0.8	0.4	1.9	0.1
MgO (wt%)	16.6	21.8	b.d.l.	2.9	0.3	15.6	19.3	18.9	0.7	0.7	3.8		0.4	0.3	0.6	0.2	0.4
CaO (wt%)	23.6	2.6	56.1	30.2	0.4	1.4	6.9	0.1	0.1	0.2	0.9		0.2	0.1	0.2	0.2	0.0
Na_2O (wt%)	0.2	0.0	0.1	0.0	0.0	0.1	1.0	0.0	0.0	0.0	0.2		0.0	0.0	0.1	0.0	0.1
K_2O (wt%)	0.0	0.2	0.0	0.0	0.0	0.1	0.6	0.0	0.0	0.0	0.2		0.0	0.0	0.0	0.0	0.0
P_2O_5 (wt%)	0.4	0.1	42.8	0.6	0.0	0.1	0.3	0.2	0.0	0.1	0.2		0.1	0.1	0.3	0.1	0.1
Total (wt%)	102.0	87.9	100.1	94.4	100.0	85.6	93.6	79.5	91.3	91.4	79.0		89.5	72.2	85.1	91.2	99.5
N (LA–ICPMS)	5	3	1	1	1	1	1	3	4	1	4	N (EPMA)	3	2	4	3	1
Sc (ppm)	**80**	**15**	**21**	**248**	**1**	**124**	**132**	**71**	**21**	**71**	**298**		**699**	**1171**	**1504**	**686**	**148**

Table 1: Average major-element and Sc contents obtained by EPMA and LA–ICPMS analysis of typical grains observed in polished sections in the different horizons of the lateritic profiles (N: number of analyses, b.d.l.: below detection limit, alt.: altered, ox.: oxide, adr: andradite, ap: apatite, bt: biotite, di: diopside, gt: goethite, hem: hematite, sme: smectite, vrm: vermiculite).

4.2. Relevance of the Parent Rock in Subsequent Scandium Concentration in Laterites

The Sc content of lateritic covers worldwide shows a correlation with the Fe concentrations (Fig. 9). The enrichment factor relative to the parent rock is similar, about ten in lateritic Sc concentrations in Australia, New Caledonia (Teitler et al., 2019) and Caribbean (Aiglsperger et al., 2016), irrespective of Sc content. These considerations suggest that the exceptional concentrations found in east Australian lateritic covers reflect, to first order, the Sc content of the parent rock. The Sc content measured in the dunitic and pyroxenitic parent rocks investigated here and observed in other widespread lithologies (Samson and Chassé, 2016) and comparisons with lateritic profiles developed above various parent lithotypes in New Caledonia (Teitler et al., 2019) indicate that Sc concentrations in lateritic profiles are expected to increase depending on the parent-rock lithotype in the following order: dunite < peridotite < gabbro/basalt < amphibolite/pyroxenite. The importance of the parent rock is also confirmed by the comparison with the transported lateritic duricrust, which has significantly lower Sc concentrations (*ca* 200 ppm) than the residual one (*ca* 500 ppm, Fig. 2). Isocon analyses (Fig. 2c) indicate that the transported material was derived from a different parent rock, poorer in Sc, explaining such differences of Sc content.

Alaskan-type ultramafic parent bodies are associated with exceptional Sc concentrations in lateritic profiles in eastern Australia. All of the highest-grade Sc deposits are developed above Paleozoic post-orogenic mafic–ultramafic intrusive complexes from the Western Volcanic Belt of the Lachlan Fold Belt in the Tasmanides (Fig. 1). These complexes, identified by aeromagnetic surveys, extend over an area limited to a few tens of kilometres. They include the Gilgai–Honeybugle, Owendale and Hylea–Bulbodney Alaskan-type ultramafic bodies, which form the respective parent rocks of the Nyngan (Ricketts and Duyvesteyn, 2018), Owendale (Moller et al., 2017) and Hylea (Gordon, 2018) Sc-rich laterites. The parent ultramafic body of the studied profiles, the Tout Intrusive Complex, is also an Alaskan-type intrusion. Its processes of formation explain the importance of such parent rocks for subsequent lateritic Sc enrichments. The Tout Intrusive Complex is formed by a concentric succession of cumulates resulting from the fractional crystallisation of a mafic magma originating from the partial fusion of a diapir of fertile upper mantle (Webb, 2014). Scandium is incompatible in the upper lithospheric mantle (Lee et al., 2005). The fertility of the mantle diapir forming the magma is thus expected to lead to high Sc contents in the resulting melt. Scandium concentrations measured in clinopyroxenes (*ca* 80 ppm) from the Tout Intrusive Complex are indeed 25 % higher than average contents reported for clinopyroxenes in global databases (Chassé et al., 2018a). The Sc content of the parent clinopyroxenite is explained by the abundance of clinopyroxenes that efficiently incorporated Sc during their crystallisation from a Sc-enriched magma. These observations support a fractional crystallisation model. Clinopyroxene, amphibole and garnet have high mineral-melt Sc partition coefficients (Tiepolo et al., 2007; Davis et al., 2013) and concentrate Sc (Chassé et al., 2018a), but only the first two phases have high enough modal abundances in common lithotypes to play a significant role in preconcentrating Sc in the parent rock cumulates of Sc-enriched lateritic profiles.

4.3. Preconcentration of Scandium by Incorporation into Smectite Under Reducing Conditions

During the early stages of weathering and formation of the saprolite and the plasmic zone, Sc is retained in the horizon of alteration (Fig. 2c). Smectite, replacing clinopyroxene, is the major Sc-bearing mineral despite the presence of Fe oxides and oxyhydroxides, known to be efficient scavengers of Sc (Chassé et al., 2017). Scandium *K*-edge XANES spectral signatures (Fig. 6) reveal that Sc is trapped through substitution in the smectite structure. The split and low-intensity pre-edge feature and the three main features visible on the edge are consistent with the incorporation of Sc into distorted octahedral sites (Chassé et al., 2018b), such as the M1 and M2 sites in smectite. Scandium substitution in the octahedral site of smectite is possible because of the similar ionic radii of octahedral Sc (0.75 Å), versus high-spin Fe(II), high-spin Fe(III) and Mg (0.78 Å, 0.65 Å and 0.72 Å, respectively). Topotactic replacement is common during the weathering of pyroxenes (Wilson, 2004). Combined with the low Sc content of near-neutral waters circulating in the saprolite (Williams-Jones and Vasyukova, 2018), this explains Sc immobilisation by substitution in smectite during its formation after clinopyroxene. Smectite is a common product of weathering of mafic–ultramafic rocks (Wilson, 2004) and also indicates poor drainage at the base of lateritic profiles (Anand and Paine, 2002). The identification of ferrous smectite ferrosaponite suggests reducing conditions. These factors limit Sc losses, in line with studies on CZ geochemistry, showing that

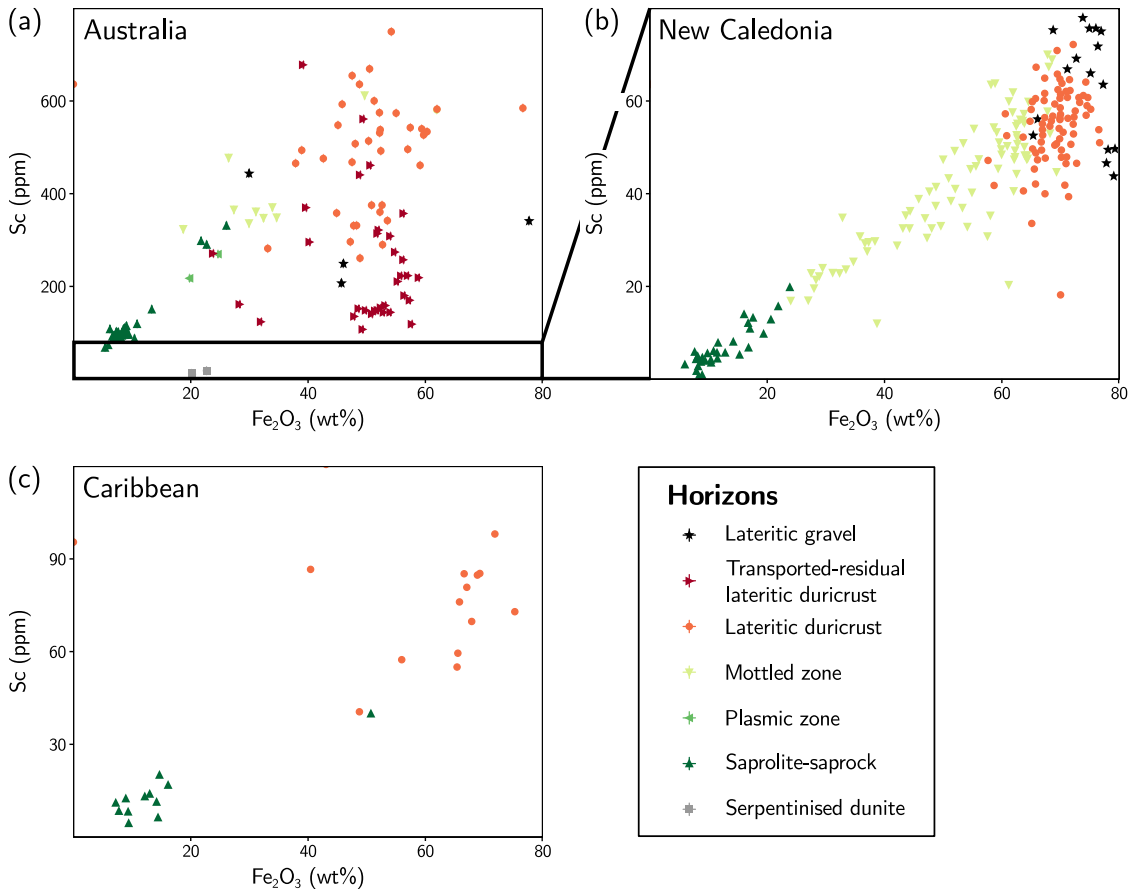

Figure 9: Scatterplot of Sc versus Fe_2O_3 contents in lateritic profiles from: (a) Syerston–Flemington, Australia (this study); (b) New Caledonia (Teitler et al., 2019); (c) Moa Bay (Cuba) and Falcondo (Dominican Republic) (Aiglsperger et al., 2016). The horizons are indicated for the Syerston–Flemington lateritic profiles; the colours for the other lateritic profiles correspond to the closest horizon, according to descriptions retrieved from the studies.

when Fe(II) is present, Sc remains immobile (Steinmann and Shotyk, 1997). The importance of smectite-rich horizons for further concentration of Sc in lateritic profiles is also supported by the presence of smectite at the base of the Sc-enriched lateritic profile at Greenvale (Zeissink, 1971).

4.4. Small-Scale and Long-Term Mechanisms Mobilising Scandium During Intense Weathering Processes

In the lateritic duricrust, isocon analyses indicate the possibility of Sc remobilisation from upper levels during intense lateritic weathering, also observed in lateritic profiles from New Caledonia (Teitler et al., 2019; Ulrich et al., 2019) and Argentina (Campodonico et al., 2019). This mobility can be explained considering smaller-scale observations. A succession of dissolution–reprecipitation reactions occurs during lateritisation, forming different generations of Fe oxides and oxyhydroxides involving variations of chemical composition. Increasing Al substitution characterises goethite ageing (Fritsch et al., 2005) and is correlated with increasing Sc content (Fig. 5a). Descending surficial waters lead to the precipitation of newly formed goethite crystals (Tardy and Nahon, 1985). This phase is the major scavenger of Sc (Chassé et al., 2017), and newly formed goethite grains concentrate Sc. This process is favoured by the decreasing solubility of Sc with increasing pH observed between upper and lower horizons (Wood and Samson, 2006; Williams-Jones and Vasyukova, 2018). The presence of Sc in the water circulating in the regolith can result from the poor affinity of Sc for hematite (Chassé et al., 2017). Scandium is expelled from goethite grains when they are replaced by hematite, as observed at the outer rims of goethite grains (Fig. 5b). Replacement of goethite by hematite is expected during periods of low water activity (Tardy and Nahon, 1985). At the top of a lateritic profile, biological inputs from the soil above can also participate in Sc release. Dissolved organic matter is indeed promoting the complexing and release of trace metals from crystalline Fe oxyhydroxides (Gadol et al., 2017). This suite of mechanisms is supported by speciation results. In bulk samples from the lateritic duricrust, Sc *K*-edge XANES spectra show that the local environment of Sc is similar to that of Sc adsorbed on mineral surfaces (Fig. 6). Weak well-resolved features indicate that only a small proportion of the Sc is substituted in Fe oxides or oxyhydroxides. Leaching experiments seem inefficient to desorb Sc from lateritic sample, as mentioned by Ulrich et al. (2019). This potential stability of the adsorption complex, preserved in such old lateritic samples, may result from the existence of an inner-sphere complex potentially associated with the inaccessibility of the adsorption surfaces. This second phenomenon would be the direct consequence of the successive dissolution–precipitation processes. During partial dissolution of Fe (oxyhydr)oxides, Sc is retained through adsorption at mineral surfaces, in particular by goethite, exhibiting higher adsorption capacity for Sc (Chassé et al., 2017). Later reprecipitation of goethite could lead to entrapment of adsorbed Sc, protecting it from desorption. These processes lead to a long-term downward mobilisation of Sc, in a slow process of continuous dissolution–precipitation, made possible by the age of the lateritic profiles, up to fifteen million years old (Metzger and Retallack, 2010).

4.5. Contrasts between Behaviours of Scandium, Rare-Earth and Conservative Elements in the Critical Zone

Despite Sc being classified as a REE (Connelly et al., 2005), this work emphasises its distinctive behaviour (Williams-Jones and Vasyukova, 2018). While Sc can be hosted by rock-forming minerals, REE are incorporated in accessory minerals in parent rocks (Braun and Pagel, 1994; Berger et al., 2014) a prerequisite for further enrichments during weathering, such as in laterites developed over carbonatites or granites (Verplanck, 2017). The first stages of supergene weathering lead to the dissolution of primary minerals and to the leaching of REE (Braun et al., 1993). The leaching of REE in the studied laterite is indicated by the negative Ce anomaly observed in the saprolite (Fig. 8). Cerium is leached from the saprolite and later oxidation to Ce^{4+} leads to its trapping in other horizons (Braun et al., 1990). Other REE remain mobile and can be redistributed in the saprolite through descending waters. In contrast to Sc, which is incorporated in major secondary clay phases, trapping of REE in the lower part of lateritic profiles is associated with adsorption onto clay minerals (Sanematsu et al., 2011; Jin et al., 2017) or concentration into accessory secondary phases (Braun et al., 1993; Berger et al., 2014). In the upper parts of the profile, REE are mobilised and redistributed downwards by descending meteoric water (Dequincey et al., 2006). Rare-earth-element patterns in the studied profiles (Fig. 8) indicate that REE are leached from the lateritic duricrust and trapped in the clay-rich plasmic zone. The positive Ce anomaly observed in the lateritic duricrust confirms this observation. Oxidised Ce^{4+} is trapped in the *cuirasse* while other REE are leached downwards. In contrast to other REE, whose maximum enrichment occurs in the plasmic zone while

they are increasingly depleted in higher-level lateritic duricrust, Sc shows maximum enrichment in the lateritic duricrust. This difference may result from the contrasted capacity of goethite to trap either REE or Sc. Rare-earth-element incorporation increases with decreasing ionic radius (Dutrizac and Soriano, 2018) but remains low compared to Sc, which can form a complete $Fe_xSc_{1-x}O(OH)$ solid solution (Levard et al., 2018). In this regard, Sc can be considered as an extremely heavy REE. The role of organic compounds in element dynamics in the studied profile may also be reflected in REE patterns. Depletion of heavy REE in higher-level lateritic duricrust is limited compared to light REE (Fig. 8). This effect can be related to the lanthanide contraction, resulting in a gradual increase of the strength of organic ligand complexation (Sonke and Salters, 2006). The similar chemical properties but smaller ionic radius of Sc can enhance complexation strength, explaining its mobilisation from upper lateritic horizons richer in organic compounds.

The pattern of elements considered as conservative in lateritic contexts (Fig. 8), such as Ti, Zr and Nb (Aiglsperger et al., 2016), indicates a continuous enrichment through the studied profiles. This is consistent with their conservative behaviour and contrasts with the geochemical behaviour of Sc in the lateritic duricrust, for which the enrichment decreases in the upper *cuirasse* horizon of the residual duricrust. The relative mobility of these immobile elements has been demonstrated for contexts of intense weathering (Du et al., 2012) or in presence of organic ligands (Cornu et al., 1999). Our results show that Sc tends to be sensitive to these effects, limiting its use as a conservative tracer during studies of tropical weathering or where complexation by organic ligands is suspected to occur.

5. Conclusions

On the basis of this work, we propose a four-stage model to account for Sc mobility and concentration during lateritic weathering (Fig. 10). (1) Preconcentration of Sc in the parent rock is made possible by accumulation of rock-forming amphibole or clinopyroxene from a Sc-rich melt and is required to form Sc-rich lateritic profiles. (2) Poor drainage at the base of lateritic profiles leads to the topotactic replacement of primary minerals in reducing conditions forming smectitic clay phases, which contain substituted Sc, immobilising this element during early weathering phases. (3) Scandium is scavenged by adsorption on goethite after clay dissolution. (4) Scandium suffers successive releasing–trapping reactions during the dissolution–crystallisation of successive generations of goethite, progressively concentrating it in the lower horizons of these old lateritic covers. Additional Sc is brought by goethite dissolution in the uppermost horizons, either assisted by organic compounds from the soil cover, or as it forms hematite in dry conditions, hence releasing Sc due to a limited affinity for hematite. As a whole, the complex structure of the CZ limits Sc dispersion relative to other elements during the development of these thick weathering profiles, preserving part of the initial Sc reservoir and giving rise to unparalleled high Sc concentrations and potential ore volumes. The similarity with laterites worldwide indicates that these processes may extend to the formation processes of lateritic profiles developed over other mafic–ultramafic rocks. This study reveals the importance of molecular-scale processes for the mobility of Sc and emphasizes the importance of speciation in deciphering the controls on element distribution in the CZ. We demonstrate the singular behaviour of Sc in this context. Unlike other REE, Sc mobility is limited during early stages of weathering. However, intense and long-term alteration eventually leads to partial remobilisation of Sc, limiting its conservative behaviour in the CZ to conditions of low-intensity weathering.

Declaration of Interest

None.

Acknowledgements

We thank Benoît Baptiste, Omar Bouddouma, Natan Capobianco, Marine Cotte, Ludovic Delbes, Michel Fialin, Thierry Pilorge, Jean-Louis Robert, Delphine Vantelon and Peter Wieland for help in sample preparation and analyses. We are also grateful to Jervois Mining Ltd for making available the drill cores. ESRF and SOLEIL facilities are acknowledged for beamtime allocation (proposal numbers 20150692 and ES426). Part of the analytical data were obtained using instrumentation funded by DEST Systemic Infrastructure Grants, ARC LIEF, NCRIS/AuScope, industry partners and Macquarie University. M. Chassé has been supported by scholarships from the École normale supérieure (ENS) and Macquarie University. This work was funded by the Institut universitaire de France (IUF) and a Foundation Grant from the ARC Centre of Excellence for Core to Crust Fluid Systems (CCFS) and Jervois Mining Ltd. This is contribution 1365 from the ARC Centre of Excellence for Core to Crust Fluid Systems (http://www.ccfs.mq.edu.au) and 1321 from the GEMOC Key Centre (http://www.gemoc.mq.edu.au).

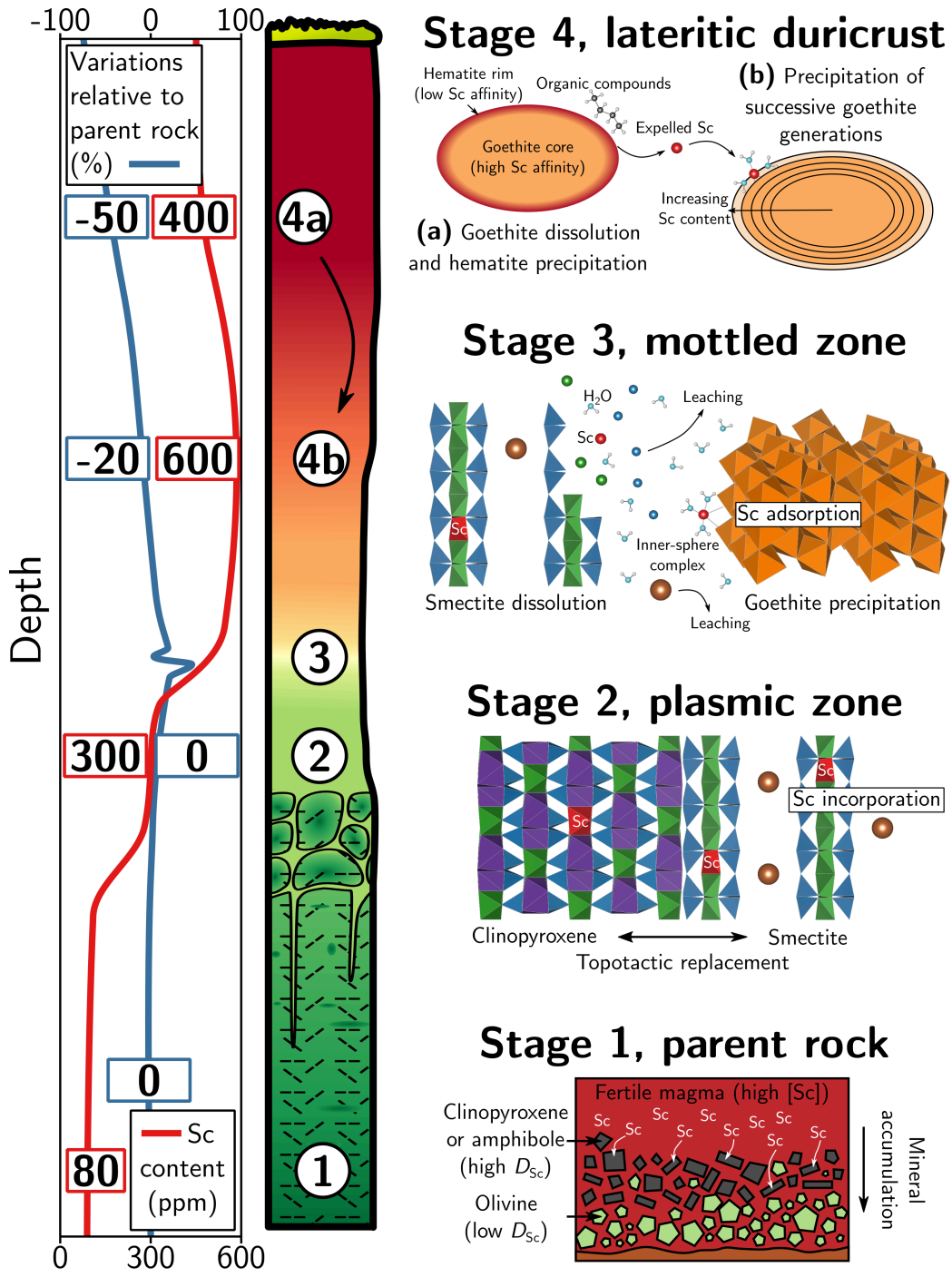

Figure 10: Four-stage model explaining Sc mobility and concentration during the formation of Sc-rich lateritic profiles. Stage 1: Scandium is preconcentrated in the parent rock by accumulation of minerals with high Sc mineral/melt partition coefficient (D_{Sc}) from a fertile magma, rich in Sc. Stage 2: Topotactic replacement of the primary phase by a smectite clay mineral in which Sc is substituted. Stage 3: Scandium is released after smectite dissolution and subsequent scavenging by adsorption on goethite through inner-sphere complex. Stage 4: Scandium is concentrated at grain boundaries between successive goethite generations, additional Sc is brought by goethite dissolution, possibly assisted by organic compounds, and through hematite replacement, this phase having a low affinity for Sc. Indicative concentrations and mass-balance values are given. The transported laterite is not represented here as it does not affect the mechanisms controlling Sc dynamics.

References

Aiglsperger T., Proenza J. A., Lewis J. F., Labrador M., Svojtka M., Rojas-Purón A., Longo F. and Durišová J. (2016) Critical Metals (REE, Sc, PGE) in Ni Laterites from Cuba and the Dominican Republic. *Ore Geol. Rev.* **73**, 127–147.

Anand R. R. and Paine M. (2002) Regolith Geology of the Yilgarn Craton, Western Australia: Implications for Exploration. *Aust. J. Earth Sci.* **49**, 3–162.

Andrew A. S., Hensen B. J., Dunlop A. C. and Agnew P. D. (1995) Oxygen and Hydrogen Isotope Evidence for the Origin of Platinum-Group Element Mineralization in Alaskan-Type Intrusions at Fifield, Australia. *Econ. Geol.* **90**, 1831–1840.

Audet M.-A. (2008) *Le massif du Koniambo, Nouvelle-Calédonie Formation et obduction d'un complexe ophiolitique du type SSZ. Enrichissement en nickel, cobalt et scandium dans les profils résiduels*. Ph. D. thesis, Université du Québec à Montréal, Canada.

Balan É., Allard T., Fritsch É., Sélo M., Falguères C., Chabaux F., Pierret M.-C. and Calas G. (2005) Formation and Evolution of Lateritic Profiles in the Middle Amazon Basin : Insights from Radiation-Induced Defects in Kaolinite. *Geochim. Cosmochim. Acta* **69**, 2193–2204.

Bell B. (2018) Quarterly Activities Report. Technical report, Australian Mines Limited, Perth, WA.

Berger A., Janots É., Gnos E., Frei R. and Bernier F. (2014) Rare Earth Element Mineralogy and Geochemistry in a Laterite Profile from Madagascar. *Appl. Geochemistry* **41**, 218–228.

Birgül O. (1981) Scandium-Iron Correlation in Clay Minerals. *Earth Planet. Sci. Lett.* **55**, 450–452.

Brantley S. L., Dibiase R. A., Russo T. A., Shi Y., Lin H., Davis K. J., Kaye M., Hill L., Kaye J., Eissenstat D. M., Hoagland B., Dere A. L., Neal A. L., Brubaker K. M. and Arthur D. K. (2016) Designing a Suite of Measurements to Understand the Critical Zone. *Earth Surf. Dyn.* **4**, 211–235.

Brantley S. L. and Lebedeva M. (2011) Learning to Read the Chemistry of Regolith to Understand the Critical Zone. *Annu. Rev. Earth Planet. Sci.* **39**, 387–416.

Braun J.-J., Muller J.-P., Bilong P., Michard A., Guillet B. and Pagel M. (1990) Cerium Anomalies in Lateritic Profiles. *Geochim. Cosmochim. Acta* **54**, 781–795.

Braun J.-J. and Pagel M. (1994) Geochemical and Mineralogical Behavior of REE, Th and U in the Akongo Lateritic Profile (SW Cameroon). *Catena* **21**, 173–177.

Braun J.-J., Pagel M., Herbillon A. J. and Rosin C. (1993) Mobilization and Redistribution of REEs and Thorium in a Syenitic Lateritic Profile: a Mass Balance Study. *Geochim. Cosmochim. Acta* **57**, 4419–4434.

Braun J.-J., Viers J., Dupré B., Polve M., Ndam J. and Muller J.-P. (1998) Solid/Liquid REE Fractionation in the Lateritic System of Goyoum, East Cameroon: the Implication for the Present Dynamics of the Soil Covers of the Humid Tropical Regions. *Geochim. Cosmochim. Acta* **62**, 273–299.

Brown D. J., Helmke P. A. and Clayton M. K. (2003) Robust Geochemical Indices for Redox and Weathering on a Granitic Laterite Landscape in Central Uganda. *Geochim. Cosmochim. Acta* **67**, 2711–2723.

Brown G. E. and Calas G. (2012) Mineral-Aqueous Solution Interfaces and Their Impact on the Environment. *Geochemical Perspect.* **1**, 483–742.

Brown G. E., Henrich V. E., Casey W. H., Clark D. L., Eggleston C., Felmy A., Goodman D. W., Grätzel M., Maciel G., McCarthy M. I., Nealson K. H., Sverjensky D. A., Toney M. F. and Zachara J. M. (1999) Metal Oxide Surfaces and Their Interactions With Aqueous Solutions and Microbial Organisms. *Chem. Rev.* **99**, 77–174.

Butt C. R. M. and Cluzel D. (2013) Nickel Laterite Ore Deposits: Weathered Serpentinites. *Elements* **9**, 123–128.

Byrne J. (2017) Annual Report. Technical report, Jervois Mining Ltd, Howthorn, Vic., Australia.

Campodonico V. A., Pasquini A. I., Lecomte K. L., García M. G. and Depetris P. J. (2019) Chemical Weathering in Subtropical Basalt-Derived Laterites: a Mass Balance Interpretation (Misiones, NE Argentina). *Catena* **173**, 352–366.

Chapela Lara M., Buss H. L. and Pett-Ridge J. C. (2018) The Effects of Lithology on Trace Element and REE Behavior During Tropical Weathering. *Chem. Geol.* **500**, 88–102.

Chassé M., Griffin W. L., Alard O., O'Reilly S. Y. and Calas G. (2018a) Insights into the Mantle Geochemistry of Scandium from a Meta-Analysis of Garnet Data. *Lithos* **310-311**, 409–421.

Chassé M., Griffin W. L., O'Reilly S. Y. and Calas G. (2017) Scandium Speciation in a World-Class Lateritic Deposit. *Geochemical Perspect. Lett.* **3**, 105–114.

Chassé M., Juhin A., Cabaret D., Delhommaye S., Vantelon D. and Calas G. (2018b) Influence of Crystallographic Environment on Scandium *K*-Edge X-Ray Absorption Near-Edge Structure Spectra. *Phys. Chem. Chem. Phys.* **20**, 23903.

Christy A. G. (2015) Causes of Anomalous Mineralogical Diversity in the Periodic Table. *Mineral. Mag.* **79**, 33–49.

Connelly N. G., Damhus T., Hartshorn R. M. and Hutton A. T. (2005) *Nomenclature of Inorganic Chemistry: IUPAC Recomendations 2005*. The Royal Society of Chemistry, Cambridge, United Kingdom.

Cornell R. M. and Schwertmann U. (2003) *The Iron Oxides — Structure, Properties, Reactions, Occurences and Uses*. Wiley-VCH, Weinheim, Germany.

Cornu S., Lucas Y., Lebon E., Ambrosi J.-P., Luizão F., Rouiller J., Bonnay M. and Neal C. (1999) Evidence of Titanium Mobility in Soil Profiles, Manaus, Central Amazonia. *Geoderma* **91**, 281–295.

Cramer J. J. and Nesbitt H. W. (1983) Mass-Balance Relations and Trace-Elements Mobility During Continental Weathering of Various Igneous Rocks. In *Pétrologue des altérations des sols. Vol III Pédologie. Pétrologie appliquée aux Subst. utiles.* Strasbourg, France. pp. 63–73.

Crawford A. J., Meffre S., Squire R., Barron L. M. and Falloon T. (2007) Middle and Late Ordovician Magmatic Evolution of the Macquarie Arc, Lachlan Orogen, New South Wales. *Aust. J. Earth Sci.* **54**, 181–214.

Das H. A., Zonderhuis J. and van der Marel H. W. (1971) Scandium in Rocks, Minerals and Sediments and Its Relations to Iron and Aluminium. *Contrib. to Mineral. Petrol.* **32**, 231–244.

Davis F. A., Humayun M., Hirschmann M. M. and Cooper R. S. (2013) Experimentally Determined Mineral/Melt Partitioning of First-Row Transition Elements (FRTE) During Partial Melting of Peridotite at 3 GPa. *Geochim. Cosmochim. Acta* **104**, 232–260.

Dequincey O., Chabaux F., Leprun J. C., Paquet H., Clauer N. and Larque P. (2006) Lanthanide and Trace Element Mobilization in a Lateritic Toposequence: Inferences from the Kaya Laterite in Burkina Faso. *Eur. J. Soil Sci.* **57**, 816–830.

Du X., Rate A. W. and Mary Gee M. A. (2012) Redistribution and Mobilization of Titanium, Zirconium and Thorium in an Intensely Weathered Lateritic Profile in Western Australia. *Chem. Geol.* **330-331**, 101–115.

Durack S. (2018) Six High-Grade Cobalt-Scandium Areas Key Focus at Granted NSW Tenement. Technical report, MinRex Resources Limited, Perth, WA.

Dutrizac J. E. and Soriano C. (2018) Behaviour of the Rare Earths During Goethite (α–FeOOH) Precipitation from Sulphate-Based Solutions. *Hydrometallurgy* **176**, 87–96.

Eshel G., Lin C. and Banin A. (2015) Novel Approach for Quantitatively Estimating Element Retention and Material Balances in Soil

Profiles of Recharge Basins Used for Wastewater Reclamation. *Sci. Total Environ.* **502**, 517–525.

Frierdich A. J., Luo Y. and Catalano J. G. (2011) Trace Element Cycling Through Iron Oxide Minerals During Redox-Driven Dynamic Recrystallization. *Geology* **39**, 1083–1086.

Fritsch É., Morin G., Bedidi A., Bonnin D., Balan É., Caquineau S. and Calas G. (2005) Transformation of Haematite and Al-Poor Goethite to Al-Rich Goethite and Associated Yellowing in a Ferralitic Clay Soil Profile of the Middle Amazon Basin (Manaus, Brazil). *Eur. J. Soil Sci.* **56**, 575–588.

Gadol H. J., Flynn E. D. and Catalano J. G. (2017) Oxalate-Promoted Trace Metal Release from Crystalline Iron Oxides Under Aerobic Conditions. *Environ. Sci. & Technol. Lett.* **4**, 311–315.

Goddéris Y. and Brantley S. L. (2013) Earthcasting the Future Critical Zone. *Elem. Sci. Anthr.* **1**, 000019.

Gordon M. (2018) Riva Resources Limited. Technical report, Independent Investment Research (Aust.) Pty Limited, Sydney, NSW, Australia.

Grant J. A. (1986) The Isocon Diagram — a Simple Solution to Gresens' Equation for Metasomatic Alteration. *Econ. Geol.* **81**, 1976–1982.

Griffin W. L., Powell W. J., Pearson N. J. and O'Reilly S. Y. (2008) GLITTER: Data Reduction Software for Laser Ablation ICP-MS. In *Laser Ablation-ICPMS Earth Sci. Curr. Pract. Outst. Issues, Vol. 40* (ed. P. Sylvester). Mineralogical Association of Canada, Vancouver, BC, Canada. pp. 307–311.

Hall G. E. M., Vaive J. E., Beer R. and Hoashi M. (1996) Selective Leaches Revisited, With Emphasis on the Amorphous Fe Oxyhydroxide Phase Extraction. *J. Geochemical Explor.* **56**, 59–78.

Jaireth S., Hoatson D. M. and Miezitis Y. (2014) Geological Setting and Resources of the Major Rare-Earth-Element Deposits in Australia. *Ore Geol. Rev.* **62**, 72–128.

Jin L., Ma L., Dere A., White T., Mathur R. and Brantley S. L. (2017) REE Mobility and Fractionation During Shale Weathering Along a Climate Gradient. *Chem. Geol.* **466**, 352–379.

Jochum K. P. and Nohl U. (2008) Reference Materials in Geochemistry and Environmental Research and the GeoReM Database. *Chem. Geol.* **253**, 50–53.

Lee C.-T. A., Leeman W. P., Canil D. and Li Z.-X. A. (2005) Similar V/Sc Systematics in MORB and Arc Basalts: Implications for the Oxygen Fugacities of Their Mantle Source Regions. *J. Petrol.* **46**, 2313–2336.

Levard C., Borschneck D., Grauby O., Rose J. and Ambrosi J.-P. (2018) Goethite, a Tailor-Made Host for the Critical Metal Scandium: the $Fe_xSc_{(1-x)}OOH$ Solid Solution. *Geochemical Perspect. Lett.* **9**, 16–20.

Maulana A., Sanematsu K. and Sakakibara M. (2016) An Overview on the Possibility of Scandium and REE Occurrence in Sulawesi, Indonesia. *Indones. J. Geosci.* **3**, 139–147.

Mehra O. P. and Jackson M. L. (1958) Iron Oxide Removal from Soils and Clays by a Dithionite-Citrate System Buffered With Sodium Bicarbonate. *Clays Clay Miner.* **7**, 317–327.

Metzger C. A. and Retallack G. J. (2010) Paleosol Record of Neogene Climate Change in the Australian Outback. *Aust. J. Earth Sci.* **57**, 871–885.

Middelburg J. J., van der Weijden C. H. and Woittiez J. R. (1988) Chemical Processes Affecting the Mobility of Major, Minor and Trace Elements During Weathering of Granitic Rocks. *Chem. Geol.* **68**, 253–273.

Moller B., Mosig R. and Hartley C. (2017) Annual Report. Technical report, Platina Resources Limited, Mt Hawthorne, WA.

Nahon D. (2003) Weathering in Tropical Zone. Significance Through Ancient and Still Active Mechanisms. *Comptes Rendus — Geosci.* **335**, 1109–1119.

Nesbitt W. H. and Markovics G. (1997) Weathering of Granodioritic Crust, Long-Term Storage of Elements in Weathering Profiles, and Petrogenesis of Siliciclastic Sediments. *Geochim. Cosmochim. Acta* **61**, 1653–1670.

Norman J. C. and Haskin L. A. (1968) The Geochemistry of Sc: a Comparision to the Rare Earths and Fe. *Geochim. Cosmochim. Acta* **32**, 93–108.

Oze C., Fendorf S., Bird D. K. and Coleman R. G. (2004) Chromium Geochemistry of Serpentine Soils. *Int. Geol. Rev.* **46**, 97–126.

Post J. E. (1999) Manganese Oxide Minerals: Crystal Structures and Economic and Environmental Significance. *Proc. Natl. Acad. Sci. U. S. A.* **96**, 3447–3453.

Ricketts N. J. and Duyvesteyn W. P. C. (2018) Scandium Recovery from the Nyngan Laterite Project in NSW. In *Light Met. 2018. TMS 2018. Miner. Met. & Mater. Ser.* (ed. O. Martin). Springer, Cham, Switzerland. pp. 1539–1543.

Rodríguez-Carvajal J. (1993) Recent Advances in Magnetic Structure Determination by Neutron Powder Diffraction. *Phys. B Condens. Matter* **192**, 55–69.

Rudnick R. L. and Gao S. (2014) Composition of the Continental Crust. In *Treatise Geochemistry, 2nd Ed.* (eds. H. Holland and K. K. Turekian), volume 4. Elsevier Ltd, Amsterdam, the Netherlands. pp. 1–51.

Salomé M., Cotte M., Baker R., Barrett R., Benseny-Cases N., Berruyer G., Bugnazet D., Castillo-Michel H., Cornu C., Fayard B., Gagliardini E., Hino R., Morse J., Papillon E., Pouyet E., Rivard C., Solé V. A., Susini J. and Veronesi G. (2013) The ID21 Scanning X-Ray Microscope at ESRF. *J. Phys. Conf. Ser.* **425**, 1–5.

Samson I. M. and Chassé M. (2016) Scandium. In *Encycl. Geochemistry* (ed. W. M. White). Springer International Publishing, Cham, Switzerland. pp. 1–5.

Sanematsu K., Moriyama T., Sotouky L. and Watanabe Y. (2011) Mobility of Rare Earth Elements in Basalt-Derived Laterite at the Bolaven Plateau, Southern Laos. *Resour. Geol.* **61**, 140–158.

Schindler M. and Hochella M. F. (2016) Nanomineralogy As a New Dimension in Understanding Elusive Geochemical Processes in Soils: the Case of Low-Solubility-Index Elements. *Geology* **44**, 515–518.

Schütz L. and Rahn K. A. (1982) Trace-Element Concentrations in Erodible Soils. *Atmos. Environ.* **16**, 171–176.

Shotyk W., Weiss D., Kramers J. D., Frei R., Cheburkin A. K., Gloor M. and Reese S. (2001) Geochemistry of the Peat Bog at Etang De La Gruère, Jura Mountains, Switzerland, and Its Record of Atmospheric Pb and Lithogenic Trace Metals (Sc, Ti, Y, Zr, and REE) Since 12,370 ^{14}C Yr BP. *Geochim. Cosmochim. Acta* **65**, 2337–2360.

Shuster D. L., Vasconcelos P. M., Heim J. A. and Farley K. A. (2005) Weathering Geochronology by (U-Th)/He Dating of Goethite. *Geochim. Cosmochim. Acta* **69**, 659–673.

Solé V. A., Papillon E., Cotte M., Walter P. and Susini J. (2007) A Multiplatform Code for the Analysis of Energy-Dispersive X-Ray Fluorescence Spectra. *Spectrochim. Acta — Part B At. Spectrosc.* **62**, 63–68.

Sonke J. E. and Salters V. J. (2006) Lanthanide-Humic Substances Complexation. I. Experimental Evidence for a Lanthanide Contraction Effect. *Geochim. Cosmochim. Acta* **70**, 1495–1506.

Steinmann P. and Shotyk W. (1997) Geochemistry, Minerology and Geochemical Mass Balance on Major Elements in Two Peat Bog Profiles (Jura Mountains, Switzerland). *Chem. Geol.* **138**, 25–53.

Sun J., Nie A.-G. and Cui T. (2017) Occurrence of a Large-Scale Scandium Deposit in Guizhou, SW China. *Boletín Técnico* **55**, 138–143.

Tardy Y. (1993) *Petrology of Laterites and Tropical Soils*. Paris, France, masson edition.

Tardy Y. and Nahon D. (1985) Geochemistry of Laterites, Stability of

Al-Goethite, Al-Hematite, and Fe^{3+}-Kaolinite in Bauxites and Ferricretes: an Approach to the Mechanism of Concretion Formation. *Am. J. Sci.* **285**, 865–903.

Teitler Y., Cathelineau M., Ulrich M., Ambrosi J.-P., Munoz M. and Sevin B. (2019) Petrology and Geochemistry of Scandium in New Caledonian Ni-Co Laterites. *J. Geochemical Explor.* **196**, 131–155.

Tiepolo M., Oberti R., Zanetti A., Vannucci R. and Foley S. F. (2007) Trace-Element Partitioning Between Amphibole and Silicate Melt. *Rev. Mineral. & Geochemistry* **67**, 417–452.

Ulrich M., Cathelineau M., Muñoz M., Boiron M.-C., Teitler Y. and Karpoff A.-M. (2019) The Relative Distribution of Critical (Sc, REE) and Transition Metals (Ni, Co, Cr, Mn, V) in Some Ni-Laterite Deposits of New Caledonia. *J. Geochemical Explor.* **197**, 93–113.

Vantelon D., Trcera N., Roy D., Moreno T., Mailly D., Guilet S., Metchalkov E., Delmotte F., Lassalle B., Lagarde P. and Flank A. M. (2016) The LUCIA Beamline at SOLEIL. *J. Synchrotron Radiat.* **23**, 635–640.

Verplanck P. L. (2017) The Role of Fluids in the Formation of Rare Earth Element Deposits. *Procedia Earth Planet. Sci.* **17**, 758–761.

Webb K. (2014) *The Age and Tectonometallogenic Setting of the Fifield "Alaskan-Type" Intrusive Suite, Lachlan Orogen, NSW*. B. Sc. thesis, University of Wollongong.

Williams-Jones A. E. and Vasyukova O. V. (2018) The Economic Geology of Scandium, the Runt of the Rare Earth Element Litter. *Econ. Geol.* **113**, 973–988.

Wilson M. J. (2004) Weathering of the Primary Rock-Forming Minerals: Processes, Products and Rates. *Clay Miner.* **39**, 233–266.

Wood S. A. and Samson I. M. (2006) The Aqueous Geochemistry of Gallium, Germanium, Indium and Scandium. *Ore Geol. Rev.* **28**, 57–102.

Zeissink H. E. (1971) Trace Element Behavior in Two Nickeliferous Laterite Profiles. *Chem. Geol.* **7**, 25–36.

Zhao M.-Y. and Zheng Y.-F. (2015) The Intensity of Chemical Weathering: Geochemical Constraints from Marine Detrital Sediments of Triassic Age in South China. *Chem. Geol.* **391**, 111–122.

Appendix A. Supplementary Material

Supplementary data associated with this article can be found in the online version.

Table EA1: Location and detailed log of the drill cores.

Table EA2: Proportion of the different mineral phases determined by Rietveld refinement for the samples from the two studied cores (abs: absent, b.d.l: below detection limit, adr: andradite, act: actinolite, ant: anatase, bhm: boehmite, cal: calcite, di: diopside, dol: dolomite, gbs: gibbsite, gt: goethite, hem: hematite, kln: kaolinite, lph: lithiophorite, mgh: maghemite, op-CT: opal-CT, qz: quartz, sme: smectite, tdk: todorokite, vrm: vermiculite).

Table EA3: Major- and trace-element concentrations measured by XRF and ICP–MS, respectively, and loss on ignition (LOI). Total weight is calculated including BaO and NiO from ICP–MS analyses.

Table EA4: Average concentrations (n: number of analyses) and standard deviations (σ) of reference materials and replicas (r = number of replicas) measured by XRF (major elements) and ICP–MS (trace elements) during whole-rock sample analyses. Preferred GeoReM values (Jochum and Nohl, 2008) are given for comparison.

Table EA5: Mass-balance calculations for major- and trace elements obtained from isocon analyses. Results are given in percentage of variation of concentration relative to the concentration in the parent rock, taken as the least altered saprock sample for each profile: JSD1–240 and JSD2–310.

Table EA6: Scandium concentrations measured by ICP–MS in the different fractions obtained after selective dissolution (AEC: adsorbed, exchangeable and carbonate, AmOx: amorphous and poorly crystalline (oxyhydr)oxides).

Table EA7: Scandium concentrations measured by ICP–MS in the solid and liquid phases recovered after experiments of Sc adsorption on goethite (Gt) or hematite (Hem) in $ScCl_3$ solutions at 10 ppm ($ScCl_3$ 10), 20 ppm ($ScCl_3$ 20), 50 ppm ($ScCl_3$ 50), 100 ppm ($ScCl_3$ 100), 200 ppm ($ScCl_3$ 200), 500 ppm ($ScCl_3$ 500) or 1000 ppm ($ScCl_3$ 1000) Sc.

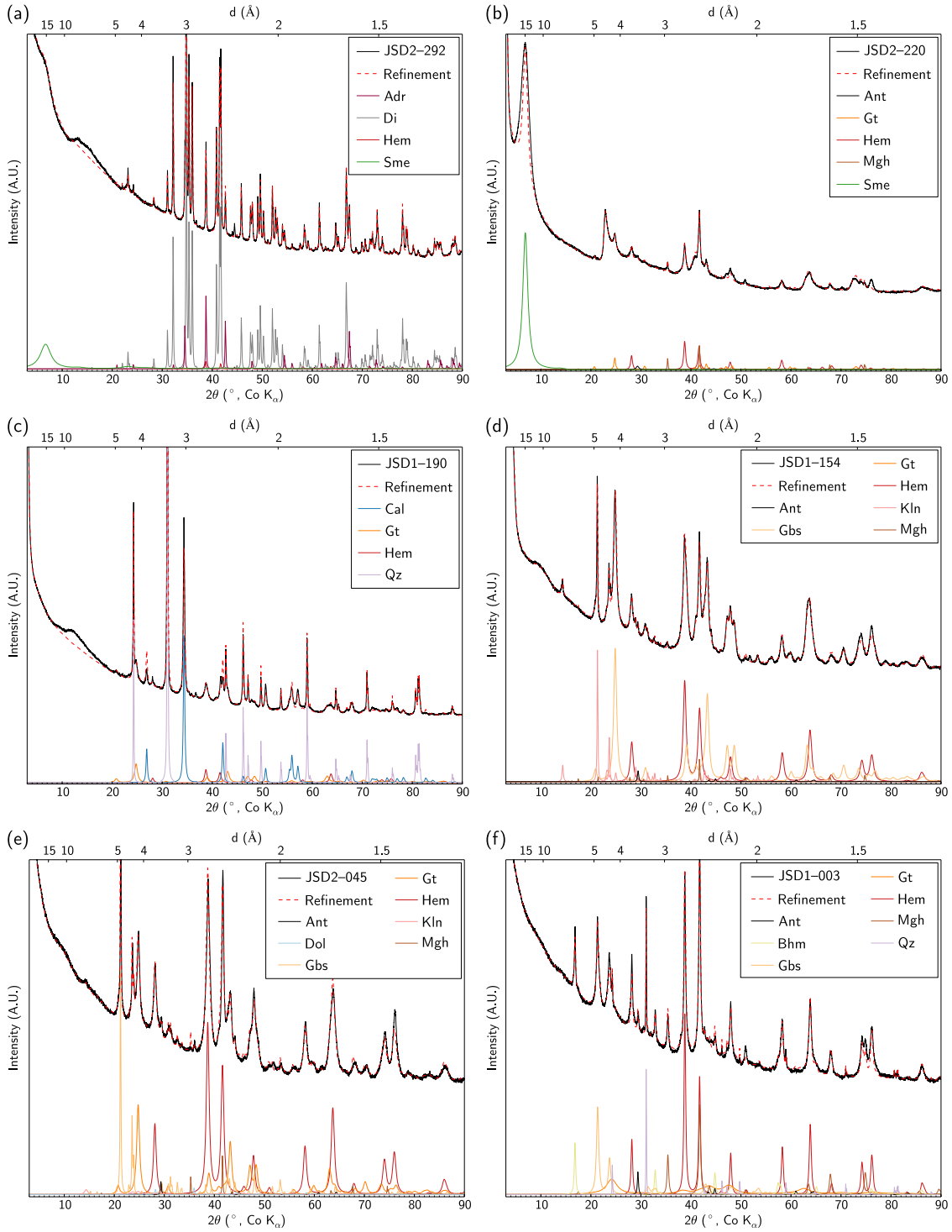

Figure EA1: Rietveld refinements of XRD patterns selected from the main different horizons and exhibiting the greatest diversity of phases: (a) saprock; (b) saprolite; (c) mottled zone; (d) lateritic duricrust; (e) transported–residual lateritic duricrust; (f) lateritic gravel. The phases refined are abbreviated as follow: adr: andradite; ant: anatase; bhm: boehmite; cal: calcite; di: diopside; dol: dolomite; gbs: gibbsite; gt: goethite; hem: hematite; kln: kaolinite; mgh: maghemite; qz: quartz; sme: smectite.

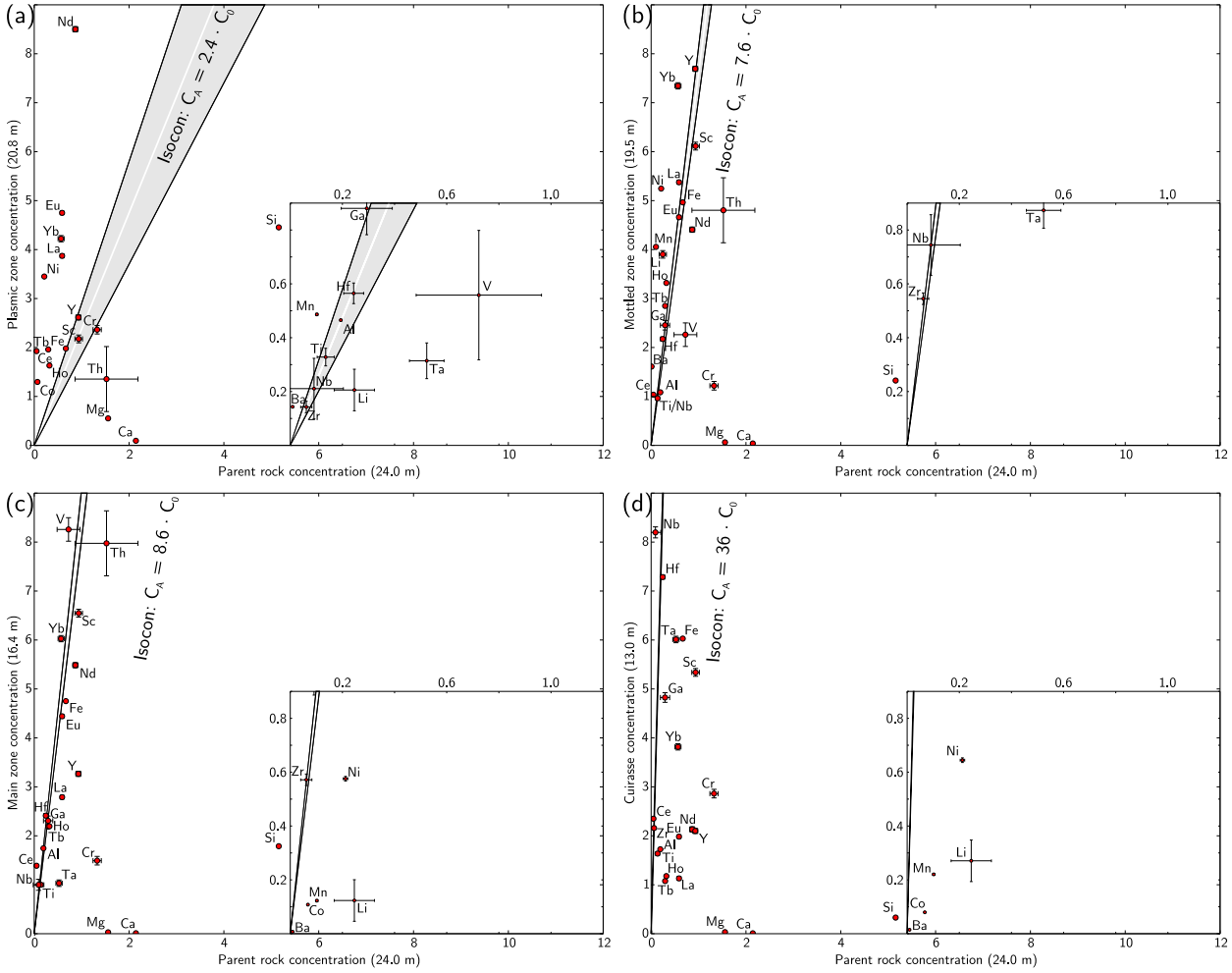

Figure EA2: Isocon diagrams for selected levels representative of different horizons of a typical lateritic profile. They give the concentrations of selected elements in an altered sample versus their concentrations in the corresponding unaltered sample. Altered samples selected are representative of the: (a) plasmic zone; (b) mottled zone; (c) main zone and (d) cuirasse. The sample least altered in the saprock has been selected to represent the concentration of the unaltered parent rock. Concentrations in Si, Al, Fe, Mg and Ca are given in wt% oxide / 10. Concentrations in Ti and Mn are given in %. Concentrations in Ba, Cr, Co and Ni are given in ‰. Concentrations in V, Zr, Ce and Sc are given in ppm / 100. Concentrations in Li, Ga, La, Nd and Y are given in ppm / 10. Concentrations in Ta and Th are given in ppm · 10. Other concentrations are given in ppm.

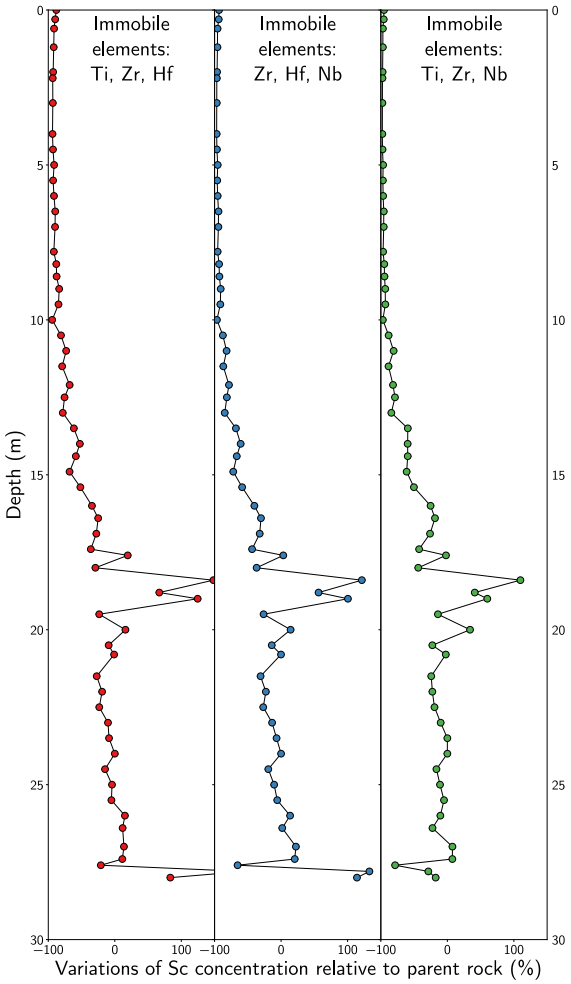

Figure EA3: Variations of the Sc concentration relative to the parent-rock concentration along a profile determined using the isocon method with distinct sets of immobile elements.